UAV Relay-Assisted Emergency Communications in IoT Networks: Resource Allocation and Trajectory Optimization

Dinh-Hieu Tran, *Student Member, IEEE*, Van-Dinh Nguyen, *Member, IEEE*, Sumit Gautam, *Member, IEEE*, Symeon Chatzinotas, *Senior Member, IEEE*, Thang X. Vu, *Member, IEEE*, and Björn Ottersten, *Fellow, IEEE*

Abstract

Unmanned aerial vehicle (UAV) communication has emerged as a prominent technology for emergency communications (e.g., natural disaster) in Internet of Things (IoT) networks to enhance the ability of disaster prediction, damage assessment, and rescue operations promptly. In this paper, a UAV is deployed as a flying base station (BS) to collect data from time-constrained IoT devices and then transfer the data to a ground gateway (GW). In general, the latency constraint at IoT users and the limited storage capacity of UAV highly hinder practical applications of UAV-assisted IoT networks. In this paper, full-duplex (FD) technique is adopted at the UAV to overcome these challenges. In addition, half-duplex (HD) scheme for UAV-based relaying is also considered to provide a comparative study between two modes (viz., FD and HD). Herein, a device is successfully served iff its data is collected by UAV and conveyed to GW within the flight time. In this context, we aim at maximizing the number of served IoT devices by jointly optimizing bandwidth and power allocation, as well as the UAV trajectory, while satisfying the requested timeout (RT) requirement of each device and the UAV's limited storage capacity. The formulated optimization problem is troublesome to solve due to its non-convexity and combinatorial nature. Toward appealing applications, we first relax binary variables into continuous values and transform the original problem into a more computationally tractable form. By leveraging inner approximation framework, we derive newly approximated functions for non-convex parts and then develop a simple yet efficient iterative algorithm for its solutions. Next, we attempt to maximize the total throughput subject to the number of served IoT devices. Finally, numerical results show that the proposed algorithms significantly outperform benchmark approaches in terms of the number of served IoT devices and the amount of collected data.

Index Terms

Emergency communications, full-duplex, information freshness, Internet-of-Things, timely data collection, unmanned aerial vehicle (UAV).

I. Introduction

In 1999, the British technology pioneer Kevin Ashton introduced a concept of the Internet-of-Things (IoT) to describe a system in which all devices with sensors are capable of connecting to each other [1]. IoT has the potential to significantly enhance the quality of human life such as smart home, health care, wearable devices, agriculture, smart city, autonomous vehicles, and smart grid [2]. The number of IoT connections of all types is estimated to reach almost 25 billions by 2025 [3]. However, the growing demand for communications is becoming a great challenge for IoT networks due to limited spectral resources at terrestrial base stations (BSs). Besides, BSs are deployed in fixed locations and antenna height to serve a fix geographical area and resources cannot be rapidly shifted elsewhere, especially, in emergency communications, whereas BSs are potentially isolated or damaged after a natural disaster, or when BSs are unable to serve all users as they are overloaded during peak hours. This raises a question of how to support the communication needs of a massive number of IoT devices with restricted resources without compromising the network performance [4]. Fortunately, due to the high maneuverability and flexible deployment, unmanned aerial vehicle (UAV) communications could become a promising technology to overcome the above shortcomings [5]. Due to energy constraints, IoT devices are commonly unable to propagate over a long distance. Thus, the UAV can fly closer to devices, harvest the IoT data, and then transmit it to the BS/control center which is out of transmission range of these devices.

Extensive studies have been carried out to investigate UAV-assisted IoT communication networks [6]–[10]. The work in [6] studied the joint optimal 3D deployment of UAVs, uplink (UL) power control, and device association in an IoT network. Specifically, the authors proposed a new framework for efficiently distributing UAVs to collect information in the UL from IoT users. In [7], the authors optimized the data gathering efficiency of a UAV-assisted IoT network, subject to the power budget, the energy capacity, and the total transmission time for IoT devices. Herein, a multi-antenna UAV was operated which followed a circular trajectory and served IoT devices to create a virtual multi-input multi-output (MIMO) channel. Reference [8] presented a robust central system orchestrator (SO) that was designed to provide value-added IoT services (VAIoTS). Whereas the SO keeps the entire details about UAVs including their current locations, flight missions, total energy budget, and their onboard IoT devices. To obtain an efficient UAV selection mechanism corresponding to each task requirement, the authors proposed three solutions, namely, energy-aware UAV, fair trade-off UAV, and delay-aware UAV selection. A novel UAV-aided IoT communication network to provide energy-efficient data gathering and accurate 3D device positioning of IoT devices was proposed in [9], whereas a UAV was deployed as an aerial anchor node and a flying

data collector. Particularly, UAVs could serve not only as aerial BSs but also as powerful IoT components that are capable of communications, sensing, and data analysis while hovering in the air [10]. Note that none of above-mentioned works in [6]–[10] take the crucial latency constraint into consideration.

Recently, the delay-sensitive data collection has attracted much attention from researchers [11]–[14]. For example, in the emergency case or during the natural disaster, the out-of-date gathering data may result in unreliable controllable decisions, which may ultimately be disastrous [14]. For example, in mission-critical IoT applications such as smart grids, factory automation (e.g., printing machines, packaging machines, and process automation), and intelligent transport systems (e.g., road safety highway and traffic efficiency) [15]. On the other hand, IoT devices often have limited storage capacity, and thus their generated data need to be collected timely before it becomes worthless due to obsolete transmissions or being overwritten by incoming data. Therefore, the UAV must reach the right place at the right time. In [11], the authors proposed two UAV trajectories, namely, the Max-AoI-optimal and Ave-AoI-optimal to efficiently collect data from ground sensor nodes under the impact of the age of information (AoI) metric. Specifically, the Max-AoI-optimal and Ave-AoI-optimal trajectory planning are to minimize the age of the oldest information and the average AoI of all sensor nodes, respectively. The work in [12] studied the role of a UAV acting as a relay to minimize the average Peak AoI for a transmitter-receiver link, which was accomplished via joint optimization of the UAV trajectory, energy spending, and the service time allocations for packet transmissions. In [13], the authors designed the UAV trajectory to minimize expired data packets in UAV-enabled wireless sensor networks (WSNs) and then applied the reinforcement learning (RL) method for the solution, which enhances the time-effectiveness and path design performance. The authors in [14] optimized the UAV trajectory as well as service bandwidth allocation to maximize the total number of served ground IoT users, in which the UAV needed to collect the data from users within their RT constraint. Different from [11]–[14], which only studied the aspect of data collection on the UL channel, the works in [16] and [17] further studied the latency constraint on the DL channel.

Despite noticeable achievements for data collection in UAV-assisted IoT networks [6]–[14], aforementioned works do not take the FD scheme into consideration. To efficiently exploit the radio spectrum, the FD transmission was adopted in UAV communications [18]–[21]. By applying a circular trajectory and decode-and-forward (DF) relaying strategy, the work [18] maximized instantaneous data rate with the joint design of beam-forming and power allocation, under individual and sum-power constraint for the source and relay users. In [19], the authors investigated the spectrum sharing planning problem for FD UAV relaying systems with underlaid device-to-device (D2D) communications which aims to maximize

the sum throughput. The work in [20] maximized the energy efficiency (EE) by jointly optimizing the UAV trajectory as well as the transmit and jamming powers of source and the UAV, respectively. Besides, a new system model for UAV-enabled FD wireless-powered IoT networks was proposed in [21]. More specifically, three optimization problems, namely, the total-time minimization, the sum-throughput maximization, and the total energy minimization problem were investigated.

Unlike previous studies such as [11]–[14], [16], [17] that only investigated the timely data exchange on the UL or DL channel utilizing HD mode, this motivates us to propose a novel system model in UAV relay-assisted IoT networks that further explores the impact of RT constraints for both the UL and DL transmission. To the best of our knowledge, this is the first work that jointly considers total bandwidth, transmission power, trajectory design, storage capacity, and latency constraint in UAV relay-assisted IoT networks. To this end, we formulate and solve two optimization problems for the new system model, and obtain some interesting observations, which would be useful for the system designers in realistic scenarios. In summary, our contributions are as follows:

- We propose a novel model in UAV relay-assisted IoT networks which takes into account the latency requirement for UL and DL channels to improve the freshness of information in emergency scenarios. Moreover, the UAV-enabled FD relaying is exploited as an effective mean to overcome UAV's limited storage capacity. In addition, UAV-enabled HD relaying is also investigated to fully capitalize on the benefits that UAV may bring to emergency communications in IoT networks5G wireless networks.
- We formulate a generalized optimization problem to maximize the total number of served IoT devices, subject to the UAV's maximum speed constraint, total traveling time constant, maximum transmit power at devices/UAV, limited cache size of UAV, and latency constraints for both UL and DL. The formulation belongs to the difficult class of mixed-integer non-convex optimization problem, which is generally NP-hard. We first relax binary variables into continuous ones and penalize the objective by an entropy-based penalty function. We then develop an iterative computational procedure for its solutions which guarantee convergence at least to local optimal. The key idea behind our approach is derive newly approximated functions for non-convex parts by employing the inner approximation (IA) framework [22].
- Inspired by the practical requirement in human safety measurements, The more the data is gathered, the better the accurate prediction can be achieved. This motivates us to investigate the optimization problem for maximizing the total collected throughput subject to a given number of served IoT users.

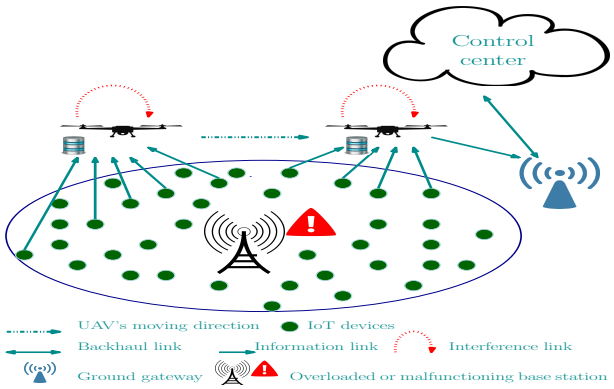

Fig. 1. System model: The ground base station (GBS) is assumed to be damaged/isolated after a natural disaster or it is overloaded during peak hours. Therefore, the UAV is deployed as a flying BS to collect the data from IoT devices and then transmit to GW.

- The effectiveness of the proposed schemes is revealed via numerical results, which show significant improvements in both numbers of served IoT devices and the total amount of collected throughput as compared with the benchmarks. More specifically, the Benchmark FD and Benchmark HD schemes are respectively designed similar to the proposed FD-based and HD-based methods but with fixed bandwidth allocation.

The rest of the paper is organized as follows. The system model and problem formulation are given in Section II. The proposed iterative algorithm for FD is presented in Section III.While, Section IV devotes for the HD scheme. Numerical results are illustrated in Section V, and Section VI concludes the paper.

Notation: Scalars and vectors are denoted by lower-case letters and boldface lower-case letters, respectively. For a set $\mathcal{K}$, $|\mathcal{K}|$ denotes its cardinality. For a vector v, $\|v\|_1$ and $\|v\|$ denote its ℓ_1 and Euclidean (ℓ_2) norm, respectively. $\mathbb{R}$ represents for the real matrix. $\mathbb{R}^+$ denotes the non-negative real numbers, i.e., $\mathbb{R}^+ = \{x \in \mathbb{R} | x \geq 0\}$. $x \sim \mathcal{CN}(0, \sigma^2)$ represents circularly symmetric complex Gaussian random variable with zero mean and variance σ^2. Finally, ∇f is the first derivative of a function f. $\mathbb{E}[x]$ denotes the expected value of x.

II. System Model and Problem Formulation

We consider a UAV-aided cooperative wireless IoT network, where a UAV is deployed to assist the existing terrestrial communication infrastructure in the case of adverse conditions or natural calamities, as shown in Fig. 1. In emergency communications, the ground base station (GBS) is either partially or completely damaged after a natural disaster, or in the case when the GBS is overloaded during the peak hours due to its incapability of handling all the devices at the same time (e.g., a sporting event) [23]. The latter case has been recognized as one of the key scenarios that need to be effectively solved by

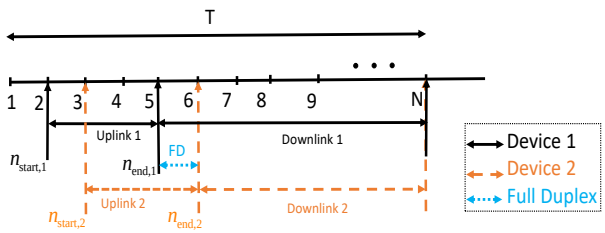

Fig. 2. Illustration of the data transmission process of 2 IoT devices with N time intervals. The first IoT device with initial data transmission time at $n_{\text{start},1} = 2$, timeout at $n_{\text{end},1} = 5$. The second IoT device with initial data transmission time at $n_{\text{start},2} = 3$, timeout at $n_{\text{end},2} = 6$. The UAV operates in the FD mode from time slots 5 to 6 since two devices utilize the same sub-carrier.

fifth-generation (5G) wireless communication [23], [24]. Concretely, a UAV helps to relay data from a set of K IoT devices (or GUs), denoted by $\mathcal{K} \triangleq \{1, \ldots, K\}$, to a GW. Each IoT device is equipped with a single antenna and works in HD mode. Due to the SWAP (size, weight, and power) limitations, the UAV, acting as an on-demand relay, is equipped with one FD antenna which can be used for data transmission and reception simultaneously. Specifically, the UAV can operate in FD or HD mode depending on the system designer. It hovers over the considered area to effectively gather data from IoT devices and then transmit to GW using UL and DL communication, respectively. Due to the limitation of the energy budget, we restrain the total serving time of UAV as T. We assume that each device is active at different time instances t, where $0 \leq t \leq T$. The location of device k is denoted as $\mathbf{r}_k \in \mathbb{R}^{2\times 1}, k \in \mathcal{K}$. We assume that the locations of IoT devices together with their data sizes, the initial data transmission time (i.e., $n_{\text{start},k}$ with $k \in \mathcal{K}$), and latency requirement (i.e., $n_{\text{end},k}$ with $k \in \mathcal{K}$) are known to the UAV through the control center.[1] Denote $n_{\text{start},k}$ and $n_{\text{end},k}$ by the initial data transmission time and timeout constraint of the device k, respectively, for $k \in \mathcal{K}$. It is assumed that the UAV should collect data from device k within $n_{\text{end},k}$ units of time. For simplicity, we assume that the UAV flies at a constant altitude of H (meters), e.g., that is imposed by the regulatory authority for safety considerations. The location of UAV projected on the ground is denoted as $q(t) \in \mathbb{R}^{2\times 1}$, with $0 \leq t \leq T$. Moreover, $\mathcal{N} = \{1, \ldots, N\}$ denotes a set of all time slots.

A. Ground-to-UAV Channel Model

For ease of exposition, the time horizon T is discretized into N equally spaced time intervals, i.e., $T = N\delta_t$ with δ_t denotes the primary slot length. Note that the location of the UAV can be assumed

[1]The control center can take care of the corresponding computations and informs the UAV through separate signaling, without affecting the performance of the considered framework [25].

to be approximately unchanged during each time slot compared to the distance from the UAV to IoT devices since δ_t is chosen sufficiently small. Then, the UAV trajectory $q(t)$ during time horizon T can be represented as $(q[n])_{n=1}^{N}$, where $q[n]$ denotes the UAV's horizontal location at n-th time interval. Let $V_{\max}$ denote the maximum velocity of the UAV, then the UAV's speed constraint can be presented as

$$\|q[n] - q[n-1]\| \leq \delta_d = V_{\max}\delta_t, n = 2, ..., N. \tag{1}$$

For notation convenience, let us denote the k-th IoT device and UAV by k, and U, respectively. Henceforth, $1k$ and $2k$ represent for the UL (i.e., $k \to \mathrm{U}$) and DL (i.e., $\mathrm{U} \to \mathrm{GW}$), respectively. Then, the time-dependence distance from $k \to \mathrm{U}$ or $\mathrm{U} \to \mathrm{GW}$ (i.e., $1k$ or $2k$), is given by

$$d_{ik}[n] = \sqrt{H^2 + \|q[n] - \mathbf{r}\|^2}, i \in \{1, 2\},\ \forall n,\ k, \tag{2}$$

where $\mathbf{r} \in \{r_k, q_0\}$, with q_0 denotes the location of GW.

In realistic scenarios, the devices are located in different environments, e.g., rural, urban, suburban, etc. Thus, a generalized channel model consisting of both the line-of-sight (LOS) and non-line-of-sight (NLOS) channel elements is considered. In this work, we consider a practical channel model that takes into account both large-scale and small-scale fading channels [26]. Specifically, the channel coefficient at the n-th time slot, $h_{ik}[n]$, can be written as [14], [27]

$$h_{ik}[n] = \sqrt{\omega_{ik}[n]}\tilde{h}_{ik}[n], \tag{3}$$

where $\omega_{ik}[n]$ represents for the large-scale fading effects and $\tilde{h}_{ik}[n]$ accounts for Rician small-scale fading coefficient. Specifically, $\omega_{ik}[n]$ can be modeled as

$$\omega_{ik}[n] = \omega_0 d_{ik}^{-\alpha}[n], \tag{4}$$

where ω_0 is the average channel power gain at the reference distance $d = 1$ meter, and $\alpha > 2$ is the path loss exponent for Rician fading channel [14]. Then, the small scale fading $\tilde{h}_{ik}[n]$ with expected value $\mathbb{E}\left[|\tilde{h}_{ik}[n]|^2\right] = 1$, is given by

$$\tilde{h}_{ik}[n] = \sqrt{\frac{G}{1+G}}\bar{h}_{ik}[n] + \sqrt{\frac{1}{1+G}}\hat{h}_{ik}[n], \tag{5}$$

where G is the Rician factor; $\bar{h}_{ik}[n]$ and $\hat{h}_{ik}[n] \sim \mathcal{CN}(0, 1)$ denote the deterministic LoS and the NLoS component (Rayleigh fading) during time slot n, respectively.

Due to the coexistence of the UL and DL channels using the same frequency at n-th time slot, the self-interference (SI) can occur at the UAV. Without loss of generality, when the UAV finishes receiving

all the data from device k, then the transmission from UAV to GW can be conducted.[2]

Let us denote by $x_{1k}[n]$ and $x_{2k}[n]$ the data symbols with unit power (i.e., $\mathbb{E}\left[|x_{1k}[n]|^2\right] = 1$ and $\mathbb{E}\left[|x_{2k}[n]|^2\right] = 1$) sent $k \to \mathrm{U}$ and $\mathrm{U} \to \mathrm{GW}$ at time slot n, respectively. We consider the transmission process for relaying the data of device k which consists of two phases: the UL from device k to UAV and the DL from UAV to GW. As a result, the received signals at the UAV and GW are respectively given by

$$y_{1k}[n] = (\sqrt{p_{1k}[n]}h_{1k}[n]x_{1k}[n] + \sqrt{\rho^{\mathrm{RSI}}}g_{\mathrm{U}}[n]\sum_{k^*\in\mathcal{K}\setminus k}\sqrt{p_{2k^*}[n]}x_{2k^*}[n] + n_0), \tag{6}$$

$$y_{2k}[n] = \sqrt{p_{2k}[n]}h_{2k}[n]x_{2k}[n] + n_0, \tag{7}$$

where RSI represents for residual self-interference term, $\rho^{\mathrm{RSI}} \in [0, 1)$ is the RSI suppression (SiS) level after interference cancellations [28]–[31], $n_0 \sim \mathcal{CN}(0, \sigma^2)$ denotes the additive white Gaussian noise (AWGN); $p_{1k}[n]$ and $p_{2k}[n]$ are the transmit power of the device k and UAV on the UL and DL to transmit the data of device k at time slot n; $g_{\mathrm{U}}[n]$ denotes the fading loop channel at UAV which interferes the UL reception due to the concurrent downlink transmission. Specifically, $g_{\mathrm{U}}[n]$ can be specified as a Rician distribution with a small factor [32], [33].

To deal with the issues involved in limited resources and the self-interference at the UAV, we consider the resources allocation (i.e., bandwidth and transmit power) for bold the UL and DL. Thus, the achievable rate (bits/s) of links from $k \to \mathrm{U}$ and $\mathrm{U} \to \mathrm{GW}$ to transmit the data of device k at time slot n are respectively given as

$$r_{1k}[n] = a_{1k}[n]B\log_2\left(1 + \Gamma_{1\mathrm{k}}\right), \tag{8}$$

$$r_{2k}[n] = a_{2k}[n]B\log_2\left(1 + \Gamma_{2\mathrm{k}}\right), \tag{9}$$

where $\Gamma_{1\mathrm{k}} \triangleq \frac{p_{1k}[n]|\tilde{h}_{1k}[n]|^2\omega_0}{\left(H^2+\|q[n]-r_k\|^2\right)^{\alpha/2}\left(\phi^{\mathrm{RSI}}\sum\limits_{k^*\in\mathcal{K}\setminus k}p_{2k^*}[n]+\sigma^2\right)}$, $\Gamma_{2\mathrm{k}} \triangleq \frac{p_{2k}[n]|\tilde{h}_{2k}[n]|^2\omega_0}{\left(H^2+\|q[n]-q_0\|^2\right)^{\alpha/2}\sigma^2}$, $\phi^{\mathrm{RSI}} \triangleq \rho^{\mathrm{RSI}}|g_{\mathrm{U}}[n]|^2$, σ^2 denotes the noise power of the AWGN; B denotes the total bandwidth in hertz (Hz) of the system; $a_{1k}[n]B$ and $a_{2k}[n]B$ are the total bandwidth allocated for the UL and DL to transmit data of k-th device during time slot n, respectively. Herein, $a_{1k}[n]$ and $a_{2k}[n]$ represent for the spectrum allocation for devices and the UAV, respectively. In practice, for a large number of resources, $a_{1k}[n]$ and $a_{2k}[n]$ are

[2]In this work, we adopt a DF relaying technique, thus, the UAV needs to complete receiving all the data from device k before relaying to GW to guarantee the data encoding properly. Moreover, a sufficiently large time period is assumed to carry out the data transfer as well as the decoding process at the UAV.

approximately continuous between 0 and 1. Thus, the bandwidth allocation should satisfy:

$$\sum_{k\in\mathcal{K}} a_{ik}[n] \leq 1, \forall n, \tag{10}$$

$$0 \leq a_{ik}[n] \leq 1, \forall k, n, \tag{11}$$

where $i \in \{1, 2\}$.

Based on (8)-(9), the throughput (in bits) received on the UL and DL to transmit the data of device k during time slot n, can respectively be written as

$$C_{1k}[n] = \delta_t R_{1k}[n], \tag{12}$$

$$C_{2k}[n] = \delta_t R_{2k}[n], \tag{13}$$

where

$$R_{1k}[n] = \begin{cases} r_{1k}[n], \text{if } n \in \mathcal{T}_{1k}, \\ 0, \qquad \text{otherwise}, \end{cases} \tag{14}$$

$$R_{2k}[n] = \begin{cases} r_{2k}[n], & \text{if } n \in \mathcal{T}_{2k}, \\ 0, & \text{otherwise}. \end{cases} \tag{15}$$

Herein, $\mathcal{T}_{1k} \triangleq \{n_{\text{start},k}, \ldots, n_{\text{end},k}\}$, $\mathcal{T}_{2k} \triangleq \{n_{\text{end},k}+1, \ldots, N\}$; (14) means that the UAV only can collect the data from device k during time period $\mathcal{T}_{1k}$. Otherwise, the data transmission rate is treated as zero. Specifically, the UAV only transmits the data of device k to GW iff it finishes the data collection process for that device, in (15). Moreover, the total throughput over N time slots received on the UL and DL are denoted as $C_{1k} = \sum\limits_{n\in\mathcal{T}_{1k}} \delta_t R_{1k}[n]$ and $C_{2k} = \sum\limits_{n\in\mathcal{T}_{2k}} \delta_t R_{2k}[n]$, respectively.

Let S_k denotes the data size (in bits) needed to transmit from device k to GW. Then, we have the RT constraint for transmitting the data of device k on the UL and DL are expressed as, respectively

$$\lambda_k \frac{S_k}{R_{1k}} \leq (n_{\text{end},k} - n_{\text{start},k})\delta_t, \forall k, \tag{16}$$

$$\lambda_k \frac{S_k}{R_{2k}} \leq (N - n_{\text{end},k})\delta_t, \forall k, \tag{17}$$

where $R_{1k} = \sum\limits_{n\in\mathcal{T}_{1k}} R_{1k}[n]$, $R_{2k} = \sum\limits_{n\in\mathcal{T}_{2k}} R_{2k}[n]$; (16) means that the device k must transmit the data to the UAV before the timeout constraint, i.e., $n_{\text{end},k}$; (17) implies that the data transmission process to transmit the data of device k from U $\rightarrow$ GW is performed during the serving time of the UAV.[3]

B. Caching Model

The UAV has a cache with storage capacity of C. Due to the limited cache size of the UAV, it can utilize FD mode to release the storage and improve the network throughput.

[3]We consider the system model in which the UAV does not transmit the data during taking off and landing [34]. Thus, the data transmission process only occurs when UAV is flying in the sky.

Considering the storage limitation, the total number of files cached at the UAV should not exceed its available storage capacity, i.e.,

$$\sum_{k\in\mathcal{K}}\left(\sum_{l=1}^{n}C_{1k}[l]-\sum_{l=1}^{n-1}C_{2k}[l]\right)\leq C, \tag{18}$$

where $\sum\limits_{l=1}^{n}C_{1k}[l]\triangleq\lambda_k S_k-\sum\limits_{l=n+1}^{N}C_{1k}[l]$.

Note that, in order to spend a part of storage capacity for future use, i.e., a free cache size to store new data streams, the amount of data stored at the UAV is calculated as the size of files collected from all devices till (n)-th time slot minus files transmitted to GW till $(n-1)$-th time slot as in (18).

C. Problem Formulation

In this section, we aim to maximize the total number of served IoT devices by jointly optimizing the UAV trajectory $q[n]$, the allocation of resources (i.e., bandwidth and transmit power assigned for UL and DL), and take into account the storage limitation, under the assumption that the locations, initial transmission time, and the timeout constraint of all the IoT devices are known a priori.

To provide assistance to the mathematical problem formulation, we introduce a new binary variable λ_k as

$$\lambda_k=\begin{cases}1, \text{Device } k \text{ is successfully served by the UAV},\\ 0, \qquad\qquad\qquad\qquad \text{otherwise.}\end{cases} \tag{19}$$

Definition 1: The value of λ_k should be equal to one iff the data intended for the k-th device is collected by the UAV, while additionally guaranteeing its successful reception at the GW.

Let us denote $\mathbf{q}=\{q[n],\forall n\}$, $\mathbf{a}=\{a_{1k}[n],a_{2k}[n],k\in\mathcal{K},n\in\mathcal{N}\}$, $\mathbf{p}=\{p_{1k}[n],p_{2k}[n],k\in\mathcal{K},n\in\mathcal{N}\}$, $\boldsymbol{\lambda}=\{\lambda_k,k\in\mathcal{K}\}$. Based on the above developments, the problem for maximizing the number of served IoT devices can be mathematically formulated as follows

$$\mathcal{P}^{\mathrm{FD}}:\max_{\mathbf{q},\mathbf{a},\mathbf{p},\boldsymbol{\lambda}}\quad \|\boldsymbol{\lambda}\|_1 \tag{20a}$$

$$\texttt{s.t.}\quad \lambda_k\in\{0,1\},\forall k,n, \tag{20b}$$

$$\delta_t\min(R_{1k},R_{2k})\geq\lambda_k S_k,\forall k, \tag{20c}$$

$$\sum_{k\in\mathcal{K}}\delta_t R_{2k}\geq\sum_{k\in\mathcal{K}}\lambda_k S_k,\forall k, \tag{20d}$$

$$\lambda_k\frac{S_k}{R_{1k}}\leq(n_{\mathrm{end},k}-n_{\mathrm{start},k})\delta_t,\forall k, \tag{20e}$$

$$\lambda_k\frac{S_k}{R_{2k}}\leq(N-n_{\mathrm{end},k})\delta_t,\forall k, \tag{20f}$$

$$\sum_{k\in\mathcal{K}}\left(\lambda_k S_k-\sum_{l=n+1}^{N}\delta_t R_{1k}[l]-\sum_{l=1}^{n-1}\delta_t R_{2k}[l]\right)\leq C,\forall n, \tag{20g}$$

$$\sum_{k\in\mathcal{K}}a_{ik}[n]\leq 1,\forall n, \tag{20h}$$

$$0\leq a_{ik}[n]\leq 1,\forall k,n, \tag{20i}$$

$$q[1] = q_I, q[N] = q_F, \tag{20j}$$

$$\|q[n] - q[n-1]\| \leq \delta_d, n = 2, \ldots, N, \tag{20k}$$

$$0 \leq p_{1k}[n] \leq P_k^{\max}[n], \forall k, n, \tag{20l}$$

$$0 \leq \sum_{k \in \mathcal{K}} p_{2k}[n] \leq P_{\mathrm{U}}^{\max}[n], \forall n, \tag{20m}$$

where constraint (20c) means that each IoT device need to upload the amount of data S_k. At the last time slot, constraint (20d) ensures that the device k is successfully served iff all the data uploaded on the UL is transmitted on the DL. Constraint (20j) explains for the beginning and ending locations of the UAV, with q_I and $q_F \in \mathbb{R}^{2\times 1}$ denote the beginning and ending locations of UAV projected onto the horizontal plane, respectively; (20k) signifies the maximum speed constraint of the UAV; constraints (20l) and (20m) imply that the total transmit power of device k and the UAV is limited by their maximum power budgets $P_k^{\max}[n]$ and $P_{\mathrm{U}}^{\max}[n]$, respectively.

The problem $\mathcal{P}^{\mathrm{FD}}$ is a mixed integer non-linear program (MINLP), which is NP-hard. Moreover, the binary constraint (20b) and the non-convex constraints (20c) to (20g) introduces intractability. Therefore, it is cumbersome to find a direct solution of $\mathcal{P}^{\mathrm{FD}}$. However, a suitable solution (local or global optimal) may be obtained by employing adequate relaxations to $\mathcal{P}^{\mathrm{FD}}$. In this regard, we provide a transformation mechanism for $\mathcal{P}^{\mathrm{FD}}$, followed by its corresponding solution in the succeeding section.

III. Proposed Iterative Algorithm for solving $\mathcal{P}^{\mathrm{FD}}$

This section provides an iterative algorithm based on the IA method to solve the design problem.

A. *Tractable Formulation for* (20)

In this section, we intend to make the problem $\mathcal{P}^{\mathrm{FD}}$ more tractable, we first relax the binary variables of (20b) into continuous values. As a result, we obtain the following optimization problem

$$\mathcal{P}_{\mathrm{relaxed}}^{\mathrm{FD}} : \max_{\mathbf{q},\mathbf{a},\mathbf{p},\boldsymbol{\lambda}} \quad \|\boldsymbol{\lambda}\|_1 \tag{21a}$$

$$\mathtt{s.t.} \quad 0 \leq \lambda_k \leq 1, \forall k, \tag{21b}$$

$$\text{(20c) to (20m) in } \mathcal{P}^{\mathrm{FD}}. \tag{21c}$$

Such a relaxation implies that the objective values of $\mathcal{P}_{\mathrm{relaxed}}^{\mathrm{FD}}$ serves as an upper bound for that of $\mathcal{P}^{\mathrm{FD}}$. Note that $\mathcal{P}_{\mathrm{relaxed}}^{\mathrm{FD}}$ is difficult to solve due to the non-convex constraints in (20c) to (20g). Noticeably, all these non-convex constraints are dependent on either $r_{1k}[n]$ or $r_{2k}[n]$. In this context, we introduce slack variables $z_{1k}[n]$ and $z_{2k}[n]$ such that $\left(H^2 + \|q[n] - r_k\|^2\right) \leq (z_{1k}[n])^{2/\alpha}$ and $\left(H^2 + \|q[n] - q_0\|^2\right) \leq (z_{2k}[n])^{2/\alpha}$, respectively, where $\alpha > 2$ for Rician fading channel [14], [35], [36], by which the (8) and (9) can be rewritten as

$$r_{1k}[n] \geq a_{1k}[n] B \log_2\Big(1 + \frac{p_{1k}[n]|\tilde{h}_{1k}[n]|^2\omega_0}{z_{1k}[n](\phi^{\mathrm{RSI}} \sum\limits_{k^*\in\mathcal{K}\setminus k} p_{2k^*}[n] + \sigma^2)}\Big), \tag{22}$$

$$r_{2k}[n] \geq r_{2k}^{\mathrm{lb}}[n] \triangleq a_{2k}[n] B \log_2\Big(1 + \frac{p_{2k}[n]|\tilde{h}_{2k}[n]|^2\omega_0}{z_{2k}[n]\sigma^2}\Big). \tag{23}$$

Herein, we note that the expression in (22) may still need some transformation to ensure tractability. Therefore, we first introduce a slack variable $t_{1k}[n]$ as a soft interference plus noise for user k during time slot n, which yields

$$(\phi^{\mathrm{RSI}} \sum_{k^*\in\mathcal{K}\setminus k} p_{2k^*}[n] + \sigma^2) \leq t_{1k}[n]. \tag{24}$$

Then, the (22) is lower bounded by

$$r_{1k}^{\mathrm{lb}}[n] = a_{1k}[n] B \log_2\Big(1 + \frac{p_{1k}[n]|\tilde{h}_{1k}[n]|^2\omega_0}{z_{1k}[n]t_{1k}[n]}\Big). \tag{25}$$

By substituting (23) and (25) into (12), (13), (14), and (15), we obtain $C_{1k}^{\mathrm{lb}}[n]$, $C_{2k}^{\mathrm{lb}}[n]$, $R_{1k}^{\mathrm{lb}}[n]$, and $R_{2k}^{\mathrm{lb}}[n]$, respectively. Moreover, we have $R_{1k}^{\mathrm{lb}} = \sum\limits_{n\in\mathcal{T}_{1k}} R_{1k}^{\mathrm{lb}}[n]$, $R_{2k}^{\mathrm{lb}} = \sum\limits_{n\in\mathcal{T}_{2k}} R_{2k}[n]$. Next, the total throughput over N time slots received on the UL and DL can be rewritten as $C_{1k}^{\mathrm{lb}} = \sum\limits_{n\in\mathcal{T}_{1k}} \delta_t R_{1k}[n]$ and $C_{2k}^{\mathrm{lb}} = \sum\limits_{n\in\mathcal{T}_{2k}} \delta_t R_{2k}[n]$, respectively. Let us denote $\mathbf{z} = \{z_{1k}[n], z_{2k}[n], n \in \mathcal{N}, k \in \mathcal{K}\}$, $\mathbf{t} = \{t_{1k}[n], k \in \mathcal{K}, n \in \mathcal{N}\}$. Then, the problem $\mathcal{P}_{\mathrm{relaxed}}^{\mathrm{FD}}$ can be reformulated as

$$\mathcal{P}_{\mathrm{relaxed},1}^{\mathrm{FD}}: \max_{\mathbf{q},\mathbf{a},\mathbf{p},\boldsymbol{\lambda},\mathbf{z},\mathbf{t}} \quad \|\boldsymbol{\lambda}\|_1 \tag{26a}$$

$$\texttt{s.t.} \quad (21\text{b}), (20\text{h}) - (20\text{m}), \tag{26b}$$

$$\Big(H^2 + \|q[n] - r_k\|^2\Big) \leq (z_{1k}[n])^{2/\alpha}, \forall k, n,$$

$$\Big(H^2 + \|q[n] - q_0\|^2\Big) \leq (z_{2k}[n])^{2/\alpha}, \forall n, \tag{26c}$$

$$(\phi^{\mathrm{RSI}} \sum_{k^*\in\mathcal{K}\setminus k} p_{2k^*}[n] + \sigma^2) \leq t_{1k}[n], \forall k, n, \tag{26d}$$

$$\lambda_k \frac{S_k}{R_{1k}^{\mathrm{lb}}} \leq (n_{\mathrm{end},k} - n_{\mathrm{start},k})\delta_t, \forall k, \tag{26e}$$

$$\lambda_k \frac{S_k}{R_{2k}^{\mathrm{lb}}} \leq (N - n_{\mathrm{end},k})\delta_t, \forall k, \tag{26f}$$

$$\delta_t \min(R_{1k}^{\mathrm{lb}}, R_{2k}^{\mathrm{lb}}) \geq \lambda_k S_k, \forall k, \tag{26g}$$

$$\sum_{k\in\mathcal{K}} \delta_t R_{2k}^{\mathrm{lb}} \geq \sum_{k\in\mathcal{K}} \lambda_k S_k, \forall k \in \mathcal{K}, \tag{26h}$$

$$\sum_{k\in\mathcal{K}} \left(\lambda_k S_k - \sum_{l=n+1}^{N} \delta_t R_{1k}[l] - \sum_{l=1}^{n-1} \delta_t R_{2k}[l]\right) \leq C, \forall k, n. \tag{26i}$$

It is noteworthy that $\mathcal{P}_{\mathrm{relaxed},1}^{\mathrm{FD}}$ is a much simpler form in comparison to $\mathcal{P}^{\mathrm{FD}}$, but the possibility of a direct solution still seem unviable. This is due to the fact that joint computations of the optimization parameters (related to (26e)-(26i)) introduces non-convexity to the problem. However, it is still possible to solve the problem in an iterative manner, with alternating optimization of the involved parameters. In the following, we discuss the above-mentioned approach in detail.

B. Proposed IA-based Algorithm

In this section, we transform (26) into a convex form. Specifically, the proposed algorithm is mainly based on the IA method [22] under which the non-convex parts are completely exposed.

Approximation of $r_{1k}^{\mathrm{lb}}[n]$ and $r_{2k}^{\mathrm{lb}}[n]$: Before proceeding further, we can express $r_{1k}^{\mathrm{lb}}[n]$ and $r_{2k}^{\mathrm{lb}}[n]$ as

$$r_{1k}^{\mathrm{lb}}[n] = a_{1k}[n]\Phi_{1k}[n], \tag{27}$$

$$r_{2k}^{\mathrm{lb}}[n] = a_{2k}[n]\Phi_{2k}[n], \tag{28}$$

where

$$\Phi_{1k}[n] = B\log_2\left(1+\frac{p_{1k}[n]|\tilde{h}_{1k}[n]|^2\omega_0}{z_{1k}[n]t_{1k}[n]}\right), \tag{29}$$

$$\Phi_{2k}[n] = B\log_2\left(1+\frac{p_{2k}[n]|\tilde{h}_{2k}[n]|^2\omega_0}{z_{2k}[n]\sigma^2}\right). \tag{30}$$

To reformulate (29) and (30) into tractable forms, we introduce the following lemmas:

Lemma 1: Consider a concave function $h(x,y) \triangleq \sqrt{xy},\ x \geq 0,\ y \geq 0$. Its upper bound at given points $x^{(j)}$ and $y^{(j)}$ can be given by [28, Appendix B], [37]

$$h(x,y) \leq \frac{\sqrt{x^{(j)}}}{2\sqrt{y^{(j)}}}y + \frac{\sqrt{y^{(j)}}}{2\sqrt{x^{(j)}}}x. \tag{31}$$

Lemma 2: Consider a function $h_1(x,y,z) \triangleq \ln\left(1+\frac{x}{yz}\right)$ and $h_2(x,z) \triangleq \ln\left(1+\frac{x}{z}\right)$. The lower bound of $h_1(x,y,z)$ and $h_2(x,z)$ at given point $x^{(j)}$, $y^{(j)}$, and $z^{(j)}$ which are expressed as

$$h_1(x,y,z) \geq \ln\left(1+\frac{x^{(j)}}{y^{(j)}z^{(j)}}\right) - \frac{x^{(j)}}{y^{(j)}z^{(j)}} + 2\frac{\sqrt{x^{(j)}}\sqrt{x}}{y^{(j)}z^{(j)}} - \frac{x^{(j)}\left(x+\frac{y^{(j)}}{2z^{(j)}}z^2+\frac{z^{(j)}}{2y^{(j)}}y^2\right)}{y^{(j)}z^{(j)}\left(x^{(j)}+y^{(j)}z^{(j)}\right)}, \tag{32}$$

$$h_2(x,z) \geq \ln\left(1+\frac{x^{(j)}}{z^{(j)}}\right) - \frac{x^{(j)}}{z^{(j)}} + 2\frac{\sqrt{x^{(j)}}\sqrt{x}}{z^{(j)}} - \frac{x^{(j)}\left(x+z\right)}{z^{(j)}\left(x^{(j)}+z^{(j)}\right)}. \tag{33}$$

Proof: See Appendix A. ■

Based on lemmas 1 and 2, $\Phi_{1k}[n]$ and $\Phi_{1k}[n]$ are lower bounded by

$$\Phi_{1k}[n] \geq \bar{\Phi}_{1k}[n] \triangleq B\Big(A_1 + A_2\big(p_{1k}[n]\big) - A_3\big(p_{1k}[n], t_{1k}[n], z_{1k}[n]\big)\Big), \tag{34}$$

$$\Phi_{2k}[n] \geq \bar{\Phi}_{2k}[n] \triangleq B\Big(C_1 + C_2\big(p_{2k}[n]\big) - C_3\big(p_{2k}[n], z_{2k}[n]\big)\Big), \tag{35}$$

where A_1, A_2, A_3, C_1, C_2, and C_3 are defined in Appendix B.

By introducing slack variables $\Phi_{1k}^{\mathrm{lb}}[n]$ and $\Phi_{1k}^{\mathrm{lb}}[n]$, we have

$$\bar{\Phi}_{1k}[n] \geq \Phi_{1k}^{\mathrm{lb}}[n], \tag{36}$$

$$\bar{\Phi}_{2k}[n] \geq \Phi_{2k}^{\mathrm{lb}}[n]. \tag{37}$$

Consequently, $r_{1k}^{\mathrm{lb}}[n]$ and $r_{2k}^{\mathrm{lb}}[n]$ are converted to the following constraints:

$$r_{1k}^{\mathrm{lb}}[n] \geq \bar{r}_{1k}^{\mathrm{lb}}[n] = a_{1k}[n]\Phi_{1k}^{\mathrm{lb}}[n], \tag{38}$$

$$r_{2k}^{\mathrm{lb}}[n] \geq \bar{r}_{2k}^{\mathrm{lb}}[n] = a_{2k}[n]\Phi_{2k}^{\mathrm{lb}}[n]. \tag{39}$$

Besides that, since $a_{1k}[n]\Phi_{1k}^{\mathrm{lb}}[n]$ and $a_{2k}[n]\Phi_{2k}^{\mathrm{lb}}[n]$ are non-convex functions. To deal with these constraints, we substitute $a_{1k}[n]\Phi_{1k}^{\mathrm{lb}}[n]$ and $a_{2k}[n]\Phi_{2k}^{\mathrm{lb}}[n]$ by equivalent Difference of Convex (DC) functions $0.25\big[(a_{1k}[n]+\Phi_{1k}^{\mathrm{lb}}[n])^2-(a_{1k}[n]-\Phi_{1k}^{\mathrm{lb}}[n])^2\big]$ and $0.25\big[(a_{2k}[n]+\Phi_{2k}^{\mathrm{lb}}[n])^2-(a_{2k}[n]-\Phi_{2k}^{\mathrm{lb}}[n])^2\big]$, respectively. Then, we apply the first-order Taylor approximation to approximate the convex functions $(a_{1k}[n]+\Phi_{1k}[n])^2$ and $(a_{2k}[n]+\Phi_{2k}[n])^2$ at the $(j+1)$-th iteration, respectively. Hence, functions $\bar{r}_{1k}^{\mathrm{lb}}[n]$ and $\bar{r}_{2k}^{\mathrm{lb}}[n]$ in (38) and (39) are respectively represented by

$$a_{1k}[n]\Phi_{1k}^{\mathrm{lb}}[n] \geq \frac{\big(a_{1k}^{(j)}[n]+\Phi_{1k}^{\mathrm{lb},(j)}[n]\big)^2}{4}+\frac{\big(a_{1k}^{(j)}[n]+\Phi_{1k}^{\mathrm{lb},(j)}[n]\big)}{2}\times\Big(a_{1k}[n]-a_{1k}^{(j)}[n]+\Phi_{1k}^{\mathrm{lb}}[n]-\Phi_{1k}^{\mathrm{lb},(j)}[n]\Big) - \frac{\big(a_{1k}[n]-\Phi_{1k}^{\mathrm{lb}}[n]\big)^2}{4} \triangleq \tilde{r}_{1k}^{\mathrm{lb}}[n], \tag{40}$$

$$a_{2k}[n]\Phi_{2k}^{\mathrm{lb}}[n] \geq \frac{\big(a_{2k}^{(j)}[n]+\Phi_{2k}^{\mathrm{lb},(j)}[n]\big)^2}{4}+\frac{\big(a_{2k}^{(j)}[n]+\Phi_{1k}^{\mathrm{lb},(j)}[n]\big)}{2}\times\Big(a_{2k}[n]-a_{2k}^{(j)}[n]+\Phi_{2k}^{\mathrm{lb}}[n]-\Phi_{2k}^{\mathrm{lb},(j)}[n]\Big) - \frac{\big(a_{2k}[n]-\Phi_{2k}^{\mathrm{lb}}[n]\big)^2}{4} \triangleq \tilde{r}_{2k}^{\mathrm{lb}}[n]. \tag{41}$$

To convexify (26e)-(26i), we introduce the slack variables $\widehat{r}_{1k}^{\mathrm{lb}}[n]$ and $\widehat{r}_{2k}^{\mathrm{lb}}[n]$, the constraints (40) and (41) are innerly approximated by the following convex constraints:

$$\tilde{r}_{1k}^{\mathrm{lb}}[n] \geq \widehat{r}_{1k}^{\mathrm{lb}}[n], \tag{42}$$

$$\tilde{r}_{2k}^{\mathrm{lb}}[n] \geq \widehat{r}_{2k}^{\mathrm{lb}}[n]. \tag{43}$$

As a result, substituting $\widehat{r}_{1k}^{\mathrm{lb}}[n]$ and $\widehat{r}_{2k}^{\mathrm{lb}}[n]$ into (12), (13), (14), and (15), we obtain $\widehat{C}_{1k}^{\mathrm{lb}}[n]$, $\widehat{C}_{2k}^{\mathrm{lb}}[n]$, $\widehat{R}_{1k}^{\mathrm{lb}}[n]$, and $\widehat{R}_{2k}^{\mathrm{lb}}[n]$, respectively. Moreover, we have $\widehat{R}_{1k}^{\mathrm{lb}}=\sum\limits_{n\in\mathcal{T}_{1k}}\widehat{R}_{1k}^{\mathrm{lb}}[n]$, $\widehat{R}_{2k}^{\mathrm{lb}}=\sum\limits_{n\in\mathcal{T}_{2k}}\widehat{R}_{2k}^{\mathrm{lb}}[n]$. Next, the total throughput over N time slots received on the UL and DL can be rewritten as $\widehat{C}_{1k}^{\mathrm{lb}}=\sum\limits_{n\in\mathcal{T}_{1k}}\delta_t\widehat{R}_{1k}^{\mathrm{lb}}[n]$ and $\widehat{C}_{2k}^{\mathrm{lb}}=\sum\limits_{n\in\mathcal{T}_{2k}}\delta_t\widehat{R}_{2k}^{\mathrm{lb}}[n]$, respectively. Let us denote $\mathbf{\Phi}=\{\Phi_{1k}^{\mathrm{lb}}[n],\Phi_{2k}^{\mathrm{lb}}[n],\forall k,n\}$ and $\mathbf{r}=\{\widehat{r}_{1k}^{\mathrm{lb}}[n],\widehat{r}_{2k}^{\mathrm{lb}}[n],\forall k,n\}$. Bearing all the above developments in mind, we solve the following approximate convex program at the $(j+1)$-th iteration:

$$\mathcal{P}_{\mathrm{convex}}: \max_{\mathbf{q},\mathbf{a},\mathbf{p},\boldsymbol{\lambda},\boldsymbol{z},\boldsymbol{t},\mathbf{\Phi},\mathbf{r},} \quad \|\boldsymbol{\lambda}\|_1 \tag{44a}$$

$$\texttt{s.t.} \quad (20\mathrm{h})-(20\mathrm{m}),(21\mathrm{b}),(26\mathrm{c}),(42),(43), \tag{44b}$$

$$\lambda_k\frac{S_k}{\widehat{R}_{1k}^{\mathrm{lb}}}\leq(n_{\mathrm{end},k}-n_{\mathrm{start},k})\delta_t,\forall k, \tag{44c}$$

$$\lambda_k\frac{S_k}{\widehat{R}_{2k}^{\mathrm{lb}}}\leq(N-n_{\mathrm{end},k})\delta_t,\forall k, \tag{44d}$$

$$\delta_t\min_K\big(\widehat{R}_{1k}^{\mathrm{lb}},\widehat{R}_{2k}^{\mathrm{lb}}\big)\geq\lambda_k S_k,\forall k, \tag{44e}$$

$$\sum_{k=1}^{K}\delta_t\widehat{R}_{2k}^{\mathrm{lb}}\geq\sum_{k=1}^{K}\lambda_k S_k, \tag{44f}$$

$$\sum_{k\in\mathcal{K}}\left(\lambda_k S_k-\sum_{l=n+1}^{N}\delta_t\widehat{R}_{1k}^{\mathrm{lb}}[l]-\sum_{l=1}^{n-1}\delta_t\widehat{R}_{2k}^{\mathrm{lb}}[l]\right)\leq C,\forall k,n. \tag{44g}$$

Algorithm 1: Proposed IA-based Iterative Algorithm to Solve (20)

Initialization: Set $j := 0$ and generate an initial feasible point $\Psi^{(0)}$ for all constraints in (48).

1: **repeat**
2: Solve (48) to obtain the optimal solution $\boldsymbol{\Psi}^\star \triangleq (\mathbf{q}^\star, \mathbf{a}^\star, \mathbf{p}^\star, \boldsymbol{\lambda}^\star, \boldsymbol{z}^\star, \boldsymbol{t}^\star, \boldsymbol{\Phi}^\star, \boldsymbol{r}^\star)$.
3: Update $\mathbf{q}^{(j+1)} := \mathbf{q}^\star, \mathbf{a}^{(j+1)} := \mathbf{a}^\star, \mathbf{p}^{(j+1)} := \mathbf{p}^\star, \boldsymbol{\lambda}^{(j+1)} := \boldsymbol{\lambda}^\star, \boldsymbol{z}^{(j+1)} := \boldsymbol{z}^\star, \boldsymbol{t}^{(j+1)} := \boldsymbol{t}^\star$.
4: Set $j := j + 1$.
5: **until** Convergence

It is observed that problem $\mathcal{P}_{\text{convex}}$ is convex since the objective and all constraints are convex, i.e., linear or quadratic constraints. Thus, it can be solved by using the standard convex optimization methods [38]. However, since the binary variable λ is relaxed to continuous values between 0 and 1 as in (21b), which does not necessarily guarantee that each value of λ_k converges to 0 or 1. This motivates us to enforce a penalty function $\mathbb{P}(\lambda_k) \triangleq \lambda_k \ln(\lambda_k) + (1 - \lambda_k) \ln(1 - \lambda_k)$, which is convex for $\lambda_k \geq 0$ [39]. Hence, the penalized reformulation of $\mathcal{P}_{\text{convex}}$ with penalty parameter $\kappa \in \mathbb{R}^+$ is expressed as,

$$\mathcal{P}^{\text{FD}}_{\text{penalty}} : \max_{\mathbf{q},\mathbf{a},\mathbf{p},\boldsymbol{\lambda},\boldsymbol{z},\boldsymbol{t},\boldsymbol{\Phi},\mathbf{r},} \quad \sum_{k\in\mathcal{K}} \Big(\lambda_k + \kappa \mathbb{P}(\lambda_k)\Big) \tag{45a}$$

$$\texttt{s.t.} \quad \text{(44a)} - \text{(44g)}. \tag{45b}$$

Particularly, the objective function in $\mathcal{P}^{\text{FD}}_{\text{penalty}}$ is a difference of concave function, i.e., $f(\lambda_k) = \sum\limits_{k\in\mathcal{K}} \Big(\lambda_k - \big(-\kappa \mathbb{P}(\lambda_k)\big)\Big)$ with convex constraints. Thus, the problem $\mathcal{P}^{\text{FD}}_{\text{penalty}}$ is a DC Programming Problem (DCP). In order to make $\mathcal{P}^{\text{FD}}_{\text{penalty}}$ become a convex problem, we replace $\mathbb{P}(\lambda_k)$ in the objective function by its first order Taylor approximation at $(j+1)$-th iteration:

$$\widehat{\mathbb{P}}(\lambda_k) \triangleq \kappa\Big(\mathbb{P}(\lambda_k^{(j)}) + \triangledown \mathbb{P}(\lambda_k^{(j)})\big(\lambda_k - \lambda_k^{(j)}\big)\Big), \tag{46}$$

where

$$\triangledown \mathbb{P}(\lambda_k^{(j)}) = \ln(\lambda_k^{(j)}) - \ln(1 - \lambda_k^{(j)}). \tag{47}$$

Motivated from above discussions, we propose an IA-based algorithm to solve problem (20) summarized in Algorithm 1. At the $(j+1)$-th iteration, it solves the following convex program (which is obtained by replacing convex part and ignoring the constant terms in the objective):

$$\mathcal{P}^{\text{FD}}_{\text{penalty},1} : \max_{\Psi} \quad \sum_{k\in\mathcal{K}} \Big(\lambda_k + \kappa \lambda_k \triangledown \mathbb{P}(\lambda_k^{(j)})\Big) \tag{48a}$$

$$\texttt{s.t.} \quad \text{(45b)}, \tag{48b}$$

where $\boldsymbol{\Psi} \triangleq \{\mathbf{q}, \mathbf{a}, \mathbf{p}, \boldsymbol{\lambda}, \mathbf{z}, \mathbf{t}, \boldsymbol{\Phi}, \mathbf{r}\}$ which correspondingly provides $\boldsymbol{\Psi}^{(j)} \triangleq \{\mathbf{q}^{(j)}, \mathbf{a}^{(j)}, \mathbf{p}^{(j)}, \boldsymbol{\lambda}^{(j)}, \mathbf{z}^{(j)}, \mathbf{t}^{(j)}, \boldsymbol{\Phi}^{(j)}, \mathbf{r}^{(j)}\}$ as the optimal solution for (48) at iteration j. To ensure the feasibility of (48) in the first run, a suitable starting point Ψ^0 should be initialized. Then, the optimal solution is obtained by successively solving (48) and updating the involved variables until satisfying the convergence condition (discussed below in detail). Finally, a pseudo-code for solving (48) is summarized in Algorithm 1.

C. Convergence and Complexity Analysis:

1) Convergence Analysis: For the sake of notational convenience, let us define the feasible set $\chi^{(j)}$ of (48) at the initiation stage of the $(j+1)$-th iteration

$$\chi^{(j)} \triangleq \{\Psi^{(j)} | \text{s.t. (44a)-(44g) are feasible } \}. \tag{49}$$

Proposition 1: The proposed Algorithm 1 yields a sequence of improved solutions converging to at least a local optimal.

Proof: To be self-contained, we briefly give the convergence analysis as follow. First, we recall that the approximate functions presented in Section III satisfy properties of the IA algorithm given in [22]. This means that the solutions for solving (48) would result in the sequences of non-decreasing objective values, i.e., $f^{(j+1)}(\lambda_k) \geq f^{(j)}(\lambda_k)$ [37, Lemma 2.2]. Moreover, the value of $f^{(j)}(\lambda_k)$ is closed and bounded due to the IA method and the power constraints (20l) and (20m). Thus, the iterative solutions of the proposed convex programs towards the Karush-Kuhn-Tucker (KKT) point are monotonically improved and converge to at least a locally optimum. ■

2) Complexity Analysis: We now provide the worst-case complexity analysis for each iteration in Algorithm 1. Since the problem (48) is convex, several solvers employing the interior point method may be applied to solve it. Thus, the number of Newton steps, denoted as N_s, is adopted to measure the worst-case complexity to obtain the solutions. Concretely, N_s can be given as [40]:

$$N_s \sim \sqrt{\text{problem size}}, \tag{50}$$

where the problem size is the total number of optimization variables. More specifically, the convex problem (48) involves $5N(1+3K)+K$ scalar real variables. As a result, the per-iteration complexity required to solve (48) is $\sqrt{5N(1+3K)+K}$. It results in the overall complexity of $N_i\sqrt{5N(1+3K)+K}$, where N_i is the number of iterations to reach a locally optimal solution.

D. Throughput Maximization:

In an emergency case or during a natural disaster, data needs to be collected promptly for assessment of the current situation in a given area. The more data is gathered, the more accurate prediction one could achieve. This motivates us to present a new problem which maximizes the total amount of collected data with a given number of served IoT devices subjected to certain quality-of-service (QoS) constraints

$$\mathcal{P}^{\mathrm{FD}}_{\mathrm{rate}}: \max_{\mathbf{q},\mathbf{a},\mathbf{p},\boldsymbol{\lambda}} \quad \sum_{k\in\mathcal{K}} \delta_t \min(R_{1k}, R_{2k}) \tag{51a}$$

$$\mathtt{s.t.} \quad \|\boldsymbol{\lambda}\|_1 \geq \lambda_{\mathrm{thresh}}, \tag{51b}$$

$$(20\mathrm{b}) - (20\mathrm{m}), \tag{51c}$$

where constraint (51c) means that the total number of served IoT devices must be greater than or equal to a predefined threshold value, i.e., $\lambda_{\mathrm{thresh}}$.

Algorithm 2: Proposed IA-based Iterative Algorithm to Solve (52)

Initialization: Set $j := 0$ and generate an initial feasible point $\Psi^{(0)}$ for all constraints in (52).

1: **repeat**
2: Solve (52) to obtain the optimal solution $\mathbf{\Psi}^\star \triangleq (\mathbf{q}^\star, \mathbf{a}^\star, \mathbf{p}^\star, \boldsymbol{\lambda}^\star, \boldsymbol{z}^\star, \boldsymbol{t}^\star, \mathbf{\Phi}^\star, \boldsymbol{r}^\star)$.
3: Update $\mathbf{q}^{(j+1)} := \mathbf{q}^\star, \mathbf{a}^{(j+1)} := \mathbf{a}^\star, \mathbf{p}^{(j+1)} := \mathbf{p}^\star, \boldsymbol{\lambda}^{(j+1)} := \boldsymbol{\lambda}^\star, \boldsymbol{z}^{(j+1)} := \boldsymbol{z}^\star, \boldsymbol{t}^{(j+1)} := \boldsymbol{t}^\star$.
4: Set $j := j + 1$.
5: **until** Convergence

Similar to $\mathcal{P}^{\mathrm{FD}}$, the problem $\mathcal{P}^{\mathrm{FD}}_{\mathrm{rate}}$ is also a MINLP, which is NP-hard. Fortunately, by applying the relaxation method as in Section III, (51) is rewritten as

$$\mathcal{P}^{\mathrm{FD}}_{\mathrm{rate,convex}}: \max_{\Psi} \quad \sum_{k\in\mathcal{K}} \delta_t \min(\widehat{R}_{1k}, \widehat{R}_{2k}) \tag{52a}$$

$$\texttt{s.t.} \quad (45\text{b}), (51\text{c}), \tag{52b}$$

where $\widehat{R}_{1k} \triangleq \widehat{R}^{\mathrm{lb}}_{1k} + \kappa\lambda_k \nabla\mathbb{P}(\lambda_k^{(j)})$, $\widehat{R}_{2k} \triangleq \widehat{R}^{\mathrm{lb}}_{2k} + \kappa\lambda_k \nabla\mathbb{P}(\lambda_k^{(j)})$, with $\widehat{R}^{\mathrm{lb}}_{1k}$ and $\widehat{R}^{\mathrm{lb}}_{2k}$ can be obtained as in Section III-B.

Consequently, the solution of problem $\mathcal{P}^{\mathrm{FD}}_{\mathrm{rate,convex}}$ can be found by successively solving a simpler convex program, as summarized in Algorithm 2.

IV. Half Duplex Mode Scheme

A. Maximizing the Number of Served IoT devices:

In order to stress the benefits of our proposed method using FD mode, we will describe again about problem by considering HD mode at UAV in this section. Then, (6) can be rewritten as

$$y^{\mathrm{HD}}_{1k}[n] = a_{1k}[n](\sqrt{p_{1k}[n]}h_{1k}[n]x_{1k}[n] + n_0). \tag{53}$$

In (53), the UAV apply HD mode, thus, it utilizes different frequencies on the UL and DL during time slot n. Consequently, the RSI is disappear compared to that of (6). Thus, the achievable rate (bits/s) of links from $k \to \mathrm{U}$ and $\mathrm{U} \to \mathrm{GW}$ to transmit the data of device k at time slot n are given as

$$r^{\mathrm{HD}}_{1k}[n] = a_{1k}[n]B\log_2\left(1 + \frac{p_{1k}[n]|\tilde{h}_{1k}[n]|^2\omega_0}{\left(H^2 + \|q[n] - r_k\|^2\right)^{\alpha/2}\sigma^2}\right), \tag{54}$$

$$r^{\mathrm{HD}}_{2k}[n] = a_{2k}[n]B\log_2\left(1 + \frac{p_{2k}[n]|\tilde{h}_{2k}[n]|^2\omega_0}{\left(H^2 + \|q[n] - r_k\|^2\right)^{\alpha/2}\sigma^2}\right). \tag{55}$$

By replacing (54) into the equations (12), (13), (14), and (15), we obtain $C^{\mathrm{HD}}_{1k}[n]$, $C^{\mathrm{HD}}_{2k}[n] = C_{2k}[n]$, $R^{\mathrm{HD}}_{1k}[n]$, and $R^{\mathrm{HD}}_{2k}[n] = R_{2k}[n]$, respectively. Then, we reformulate the problem of maximizing the total number of served IoT devices as follows

$$\mathcal{P}^{\mathrm{HD}}: \max_{\mathbf{q},\mathbf{a},\mathbf{p},\boldsymbol{\lambda}} \quad \|\boldsymbol{\lambda}\|_1 \tag{56a}$$

$$\texttt{s.t.} \quad (20\text{b}), (20\text{d}), (20\text{f}), (20\text{h}) - (20\text{m}), \text{ in } \mathcal{P}^{\mathrm{FD}}, \tag{56b}$$

$$\delta_t \min(R_{1k}^{\mathrm{HD}}, R_{2k}) \geq \lambda_k S_k, \forall k, \tag{56c}$$

$$\lambda_k \frac{S_k}{R_{1k}} \leq (n_{\mathrm{end},k} - n_{\mathrm{start},k})\delta_t, \forall k, \tag{56d}$$

$$\sum_{k\in\mathcal{K}} \left(\lambda_k S_k - \sum_{l=n+1}^{N} \delta_t R_{1k}[l] - \sum_{l=1}^{n-1} \delta_t R_{2k}[l] \right) \leq C, \forall n. \tag{56e}$$

The problem $\mathcal{P}^{\mathrm{HD}}$ is non-convex because the binary constraint (20b) and other non-convex constraints (20d), (20f), (56c), (56d), and (56e). In order to seek a suitable solution, we first relax the binary constraint (20b) as in (26b). Then, by introducing $z_{1k}^{\mathrm{HD}}[n]$ and $z_{2k}^{\mathrm{HD}}[n]$ such that $\left(H^2 + \|q[n] - r_k\|^2\right) \leq (z_{1k}^{\mathrm{HD}}[n])^{2/\alpha}$ and $\left(H^2 + \|q[n] - q_0\|^2\right) \leq (z_{2k}^{\mathrm{HD}}[n])^{2/\alpha}$, respectively, with $\alpha > 2$ for Rician fading channel [14], [35], [36], by which the (54) and (55) can be expressed as

$$r_{1k}^{\mathrm{HD}}[n] = a_{1k}[n] B \log_2 \left(1 + \frac{p_{1k}[n]|\tilde{h}_{1k}[n]|^2 \omega_0}{z_{1k}^{\mathrm{HD}}[n]\sigma^2} \right), \tag{57}$$

$$r_{2k}^{\mathrm{HD}}[n] = a_{2k}[n] B \log_2 \left(1 + \frac{p_{2k}[n]|\tilde{h}_{2k}[n]|^2 \omega_0}{z_{2k}^{\mathrm{HD}}[n]\sigma^2} \right). \tag{58}$$

It is easy to see that the $r_{1k}^{\mathrm{HD}}[n]$ and $r_{2k}^{\mathrm{HD}}[n]$ are totally the same as $r_{2k}^{\mathrm{lb}}[n]$ in (23). Thus, we can apply the IA method for $r_{2k}^{\mathrm{lb}}[n]$ in Section III to $r_{1k}^{\mathrm{HD}}[n]$ and $r_{2k}^{\mathrm{HD}}[n]$. As a result, $r_{1k}^{\mathrm{HD}}[n]$ and $r_{2k}^{\mathrm{HD}}[n]$ can be rewritten as

$$r_{1k}^{\mathrm{HD}}[n] = a_{1k}[n]\Phi_{1k}^{\mathrm{HD}}[n], \tag{59}$$

$$r_{2k}^{\mathrm{HD}}[n] = a_{2k}[n]\Phi_{2k}^{\mathrm{HD}}[n], \tag{60}$$

where

$$\Phi_{1k}^{\mathrm{HD}}[n] = B \log_2 \left(1 + \frac{p_{1k}[n]|\tilde{h}_{1k}[n]|^2 \omega_0}{z_{1k}^{\mathrm{HD}}[n] t_{1k}[n]} \right), \tag{61}$$

$$\Phi_{2k}^{\mathrm{HD}}[n] = B \log_2 \left(1 + \frac{p_{2k}[n]|\tilde{h}_{2k}[n]|^2 \omega_0}{z_{2k}^{\mathrm{HD}}[n]\sigma^2} \right). \tag{62}$$

Similar to (35), $\Phi_{1k}[n]$ and $\Phi_{1k}[n]$ are lower bounded by

$$\Phi_{1k}^{\mathrm{HD}}[n] \geq \bar{\Phi}_{1k}^{\mathrm{HD}}[n], \tag{63}$$

$$\Phi_{2k}^{\mathrm{HD}}[n] \geq \bar{\Phi}_{2k}^{\mathrm{HD}}[n], \tag{64}$$

where $\bar{\Phi}_{1k}^{\mathrm{HD}}[n]$ and $\bar{\Phi}_{1k}^{\mathrm{HD}}[n]$ can be calculated as $\bar{\Phi}_{2k}[n]$, see Appendix B.

As in (38) and (39), it follows that

$$r_{1k}^{\mathrm{HD}}[n] \geq r_{1k}^{\mathrm{HD,lb}}[n] = a_{1k}[n]\Phi_{1k}^{\mathrm{HD,lb}}[n], \tag{65}$$

$$r_{2k}^{\mathrm{HD}}[n] \geq r_{2k}^{\mathrm{HD,lb}}[n] = a_{2k}[n]\Phi_{2k}^{\mathrm{HD,lb}}[n], \tag{66}$$

where $\Phi_{1k}^{\mathrm{HD,lb}}[n]$ and $\Phi_{2k}^{\mathrm{HD,lb}}[n]$ are new slack variables which are lower bound of $\bar{\Phi}_{1k}^{\mathrm{HD}}[n]$ and $\bar{\Phi}_{2k}^{\mathrm{HD}}[n]$, respectively. Then, we apply the first order Taylor approximation for $a_{1k}[n]\Phi_{1k}^{\mathrm{HD,lb}}[n]$ and $a_{2k}[n]\Phi_{2k}^{\mathrm{HD,lb}}[n]$, it yields to

Algorithm 3: Proposed IA-based Iterative Algorithm to Solve (71)

Initialization: Set $j := 0$ and generate an initial feasible point $\Psi^{(0)}$ for all constraints in (71).

1: **repeat**
2: Solve (71) to obtain the optimal solution $\boldsymbol{\Psi}^\star \triangleq (\mathbf{q}^\star, \mathbf{a}^\star, \mathbf{p}^\star, \boldsymbol{\lambda}^\star, \boldsymbol{z}^\star, \boldsymbol{\Phi}^\star, \boldsymbol{r}^\star)$.
3: Update $\mathbf{q}^{(j+1)} := \mathbf{q}^\star, \mathbf{a}^{(j+1)} := \mathbf{a}^\star, \mathbf{p}^{(j+1)} := \mathbf{p}^\star, \boldsymbol{\lambda}^{(j+1)} := \boldsymbol{\lambda}^\star, \boldsymbol{z}^{(j+1)} := \boldsymbol{z}^\star$.
4: **until** Convergence

$$r_{1k}^{\mathrm{HD,lb}}[n] \geq \bar{r}_{1k}^{\mathrm{HD,lb}}[n], \tag{67}$$

$$r_{2k}^{\mathrm{HD,lb}}[n] \geq \bar{r}_{2k}^{\mathrm{HD,lb}}[n], \tag{68}$$

where $\bar{r}_{1k}^{\mathrm{HD,lb}}[n]$ and $\bar{r}_{2k}^{\mathrm{HD,lb}}[n]$ can be represented as in RHS of (40) and (41), respectively.

In turn, by introducing slack variables $\widehat{r}_{1k}^{\mathrm{HD,lb}}[n]$ and $\widehat{r}_{2k}^{\mathrm{HD,lb}}[n]$, the constraints (67) and (68) are innerly approximated by the following convex constraints:

$$\bar{r}_{1k}^{\mathrm{HD,lb}}[n] \geq \widehat{r}_{1k}^{\mathrm{HD,lb}}[n], \tag{69}$$

$$\bar{r}_{2k}^{\mathrm{HD,lb}}[n] \geq \widehat{r}_{2k}^{\mathrm{HD,lb}}[n]. \tag{70}$$

In Algorithm 3, we propose an Iterative algorithm to solve the problem (56). At the j-th iteration, it solves the following convex program:

$$\mathcal{P}_{\mathrm{convex}}^{\mathrm{HD}}: \max_{\Psi} \quad \sum_{k\in\mathcal{K}} \left(\lambda_k + \kappa\lambda_k \nabla \mathbb{P}(\lambda_k^{(j)})\right) \tag{71a}$$

$$\texttt{s.t.} \quad (20\text{b}), (20\text{d}), (20\text{f}), (20\text{h}) - (20\text{m}), (69), (70), \tag{71b}$$

$$\delta_t \min(\bar{R}_{1k}^{\mathrm{HD,lb}}, \bar{R}_{2k}^{\mathrm{HD,lb}}) \geq \lambda_k S_k, \forall k, \tag{71c}$$

$$\lambda_k \frac{S_k}{\bar{R}_{1k}^{\mathrm{HD,lb}}} \leq (n_{\mathrm{end},k} - n_{\mathrm{start},k})\delta_t, \forall k, \tag{71d}$$

$$\sum_{k\in\mathcal{K}} \left(\lambda_k S_k - \sum_{l=n+1}^{N} \delta_t \bar{R}_{1k}^{\mathrm{HD,lb}}[l] - \sum_{l=1}^{n-1} \delta_t \bar{R}_{2k}^{\mathrm{HD,lb}}[l]\right) \leq C, \forall n. \tag{71e}$$

Specifically, similar to (45), we adopt the penalty function in the objective to guarantee the convergence of λ_k value to either 0 or 1, $\forall k \in \mathcal{K}$.

1) Complexity Analysis: : The convex problem (71) involves $3N(1+4K)+K$ scalar real variables. As a result, the per-iteration complexity required to solve (71) is $\sqrt{3N(1+4K)+K}$. It results in the overall complexity is $N_i\sqrt{3N(1+4K)+K}$, with N_i is the number of iterations to reach a local solution.

Remark 1: It is noteworthy that any feasible solution for (71) is also a feasible solution of problem (48) but not vice versa because the result obtained for (48) is the upper bound for the one in (71). It can be explained by the fact that the problem (71) only considers HD mode at UAV to mitigate the interference which also restricts the spectrum efficiency. The more spectrum allocation of the downlink

Algorithm 4: Proposed IA-based Iterative Algorithm to Solve (72)

Initialization: Set $j := 0$ and generate an initial feasible point $\Psi^{(0)}$ for all constraints in (72).

1: **repeat**
2: Solve (72) to obtain the optimal solution $\boldsymbol{\Psi}^\star \triangleq (\mathbf{q}^\star, \mathbf{a}^\star, \mathbf{p}^\star, \boldsymbol{\lambda}^\star, \boldsymbol{z}^\star, \boldsymbol{\Phi}^\star, \boldsymbol{r}^\star)$.
3: Update $\mathbf{q}^{(j+1)} := \mathbf{q}^\star, \mathbf{a}^{(j+1)} := \mathbf{a}^\star, \mathbf{p}^{(j+1)} := \mathbf{p}^\star, \boldsymbol{\lambda}^{(j+1)} := \boldsymbol{\lambda}^\star, \boldsymbol{z}^{(j+1)} := \boldsymbol{z}^\star$.
4: Set $j := j + 1$.
5: **until** Convergence

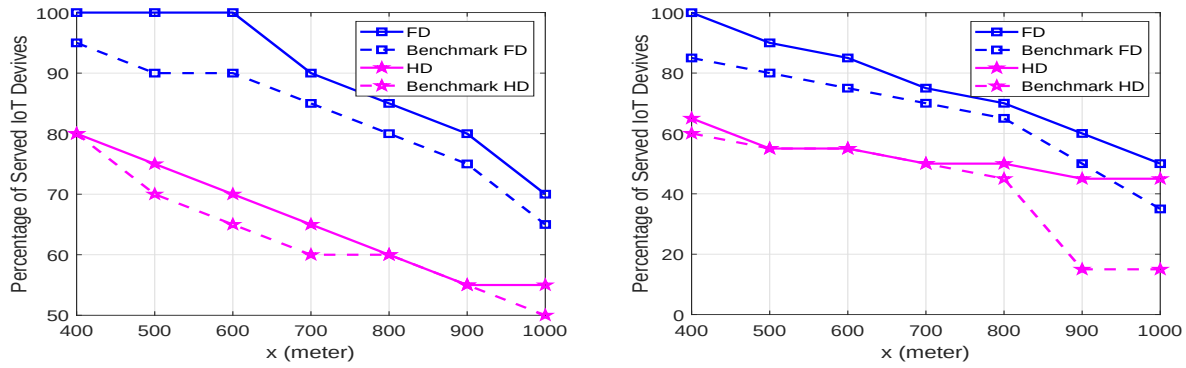

(a) N = 70 (b) N = 60

Fig. 3. Percentage of served devices vs. network size.

from U $\rightarrow$ GW is, the more successfully served IoT devices can be retrieved. This remark will be taken up further in the simulation results.

B. Throughput Maximization:

In this section, we reuse all the slack variable definitions as introduced in Sections III-D and IV-A. By following the same steps presented in Section III-D, we obtain the following tractable optimization problem

$$\mathcal{P}_{\text{rate}}^{\text{HD}}: \max_{\Psi} \quad \sum_{k\in\mathcal{K}} \delta_t \min(\bar{R}_{1k}^{\text{HD}}, \bar{R}_{2k}^{\text{HD}}) \tag{72a}$$

$$\texttt{s.t.} \quad (71\text{b}), (71\text{c}), (71\text{d}), (71\text{e}), (51\text{c}), \tag{72b}$$

where $\bar{R}_{1k}^{\text{HD}} \triangleq \bar{R}_{1k}^{\text{HD,lb}} + \kappa\lambda_k \nabla\mathbb{P}(\lambda_k^{(j)})$, $\bar{R}_{2k}^{\text{HD}} \triangleq \bar{R}_{2k}^{\text{HD,lb}} + \kappa\lambda_k \nabla\mathbb{P}(\lambda_k^{(j)})$, while $\bar{R}_{1k}^{\text{HD,lb}}$ and $\bar{R}_{2k}^{\text{HD,lb}}$ can be obtained as in Section IV. Due to the convexity of problem $\mathcal{P}_{\text{rate}}^{\text{HD}}$, the solution of problem $\mathcal{P}_{\text{rate}}^{\text{HD}}$ can be iteratively obtained as in Algorithm 4.

V. Numerical Results

In this section, we present the numerical results to evaluate the proposed joint bandwidth allocation and transmit power for the devices/UAV as well as the UAV trajectory design in UAV-assisted IoT networks.

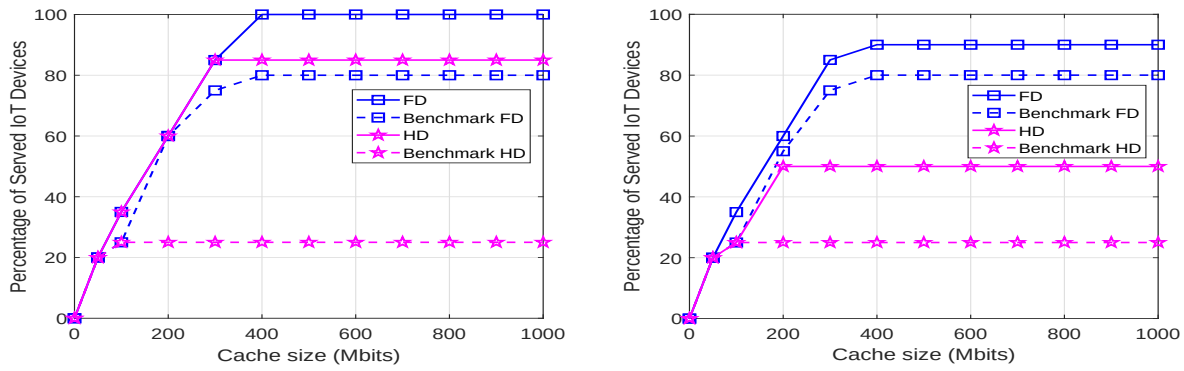

(a) $r_{\text{thresh}} = 1$ (b) $r_{\text{thresh}} = 2.8$

Fig. 4. Percentage of served devices vs. cache size with different QoS requirement.

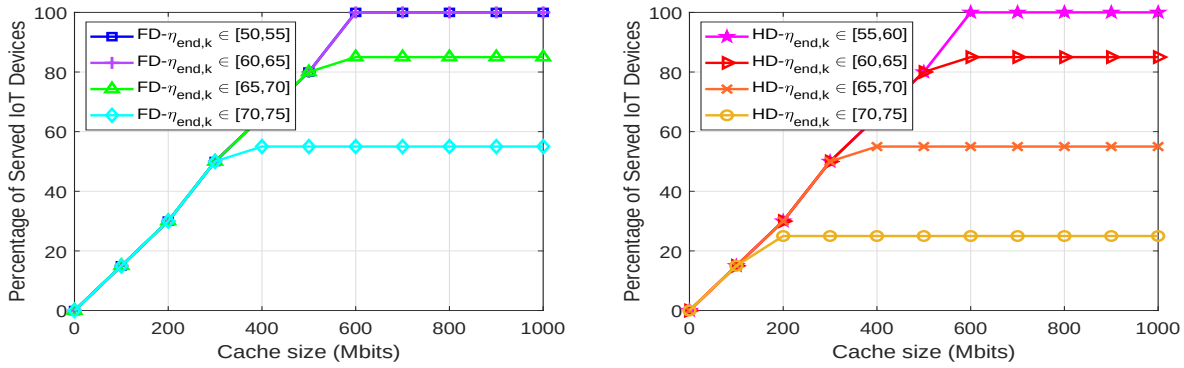

(a) Full-duplex mode (b) Half-duplex mode

Fig. 5. Percentage of served devices vs. cache size with different range of $\eta_{\text{end,k}}$.

We consider a system with K IoT devices that are randomly distributed in a horizontal plane,i.e, 500 meters x 500 meters. We assume that the GW, the start location, and end location of the UAV are located at (0, 500 meters), q_I = [300 meters, 200 meters], and q_F = [100 meters, 0], respectively. The UAV flight altitude is invariant at $H = 100$ meters [41]. The total bandwidth is $B = 10$ MHz. The transmit power budget of the UAV and IoT devices is respectively set as $P_U^{\max} = 20$ dBm and $P_k^{\max} = 15$ dBm. Other parameters are set as follows: path loss exponent $\alpha = 2.3$, $\sigma^2 = -110$ dBm, ω_0 = -40 dB, $S_k = 30$ Mbits, Rician factor G = 12 dB, the maximum collection time deadline for each device k $n_{\text{end},k}$ is uniformly distributed between $n_{\text{end},k}^{\min}$ and $n_{\text{end},k}^{\max}$. To show the superiority of our designs, we compare proposed methods with benchmark schemes. Herein, the Benchmark FD and Benchmark HD are respectively implemented similar to Algorithms 1 and 2 with fixed values of $\mathbf{a}$, i.e., $a_{1k}[n] = a_{1k}[n] = \frac{B}{K}$.

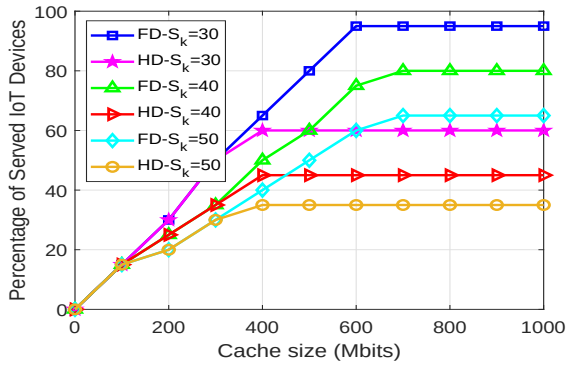

Fig. 6. Percentage of served devices vs. cache sizes.

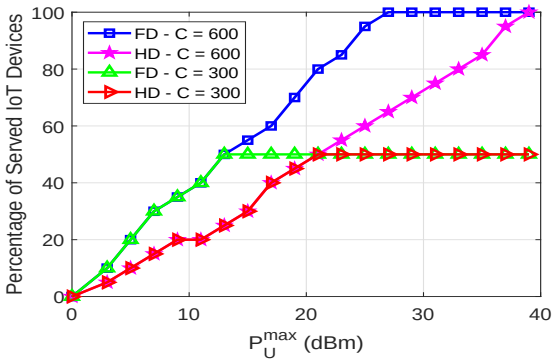

Fig. 7. Percentage of served devices vs. $P_U^{\max}$.

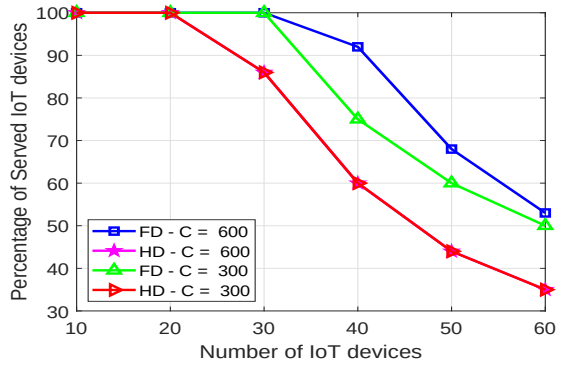

(a) Different cache size, S_k = 10 Mbits.

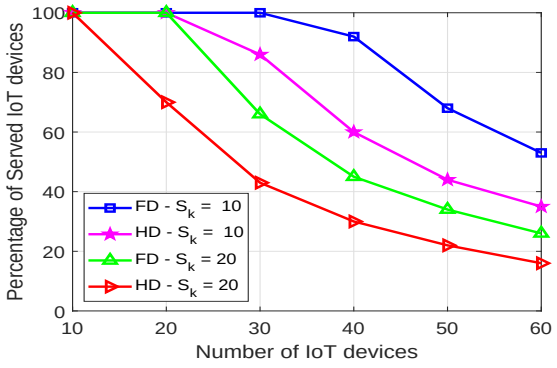

(b) Different data size, C = 600 Mbits.

Fig. 8. Percentage of served devices vs. number of IoT devices.

A. Maximizing the Number of Served IoT devices:

Fig. 3 evaluates the percentage of served devices versus network size, i.e., x (meters), with $K = 20$, while the UAV's horizontal area is calculated as: $\text{area} = x^2\ (m^2)$. As illustrated, the larger network size is, the fewer devices can be successfully served. The reason is because the IoT devices are distributed in a larger area. Thus, providing more speed is required to fulfill the GUs' latency requirement, but the $V_{\max}$ is limited. Furthermore, by increasing total traveling time N also improves the performance. It is due to the fact that the UAV has more time to exchange information with the IoT devices and GW. It is also shown that the proposed FD method significantly improves the number of served IoT devices compared with the HD method for all values of x (meter). Because in FD mode, the UAV transfers data of device k to ground gateway right after it finishes gathering data of that IoT device. While in HD mode, the UAV only operates in the downlink transmission when it completes the data acquisition for all users on the uplink to prevent RSI at the UAV. Consequently, FD scheme has a higher probability of satisfying the GUs' RT. Besides, the Benchmark FD and Benchmark HD schemes can be considered as

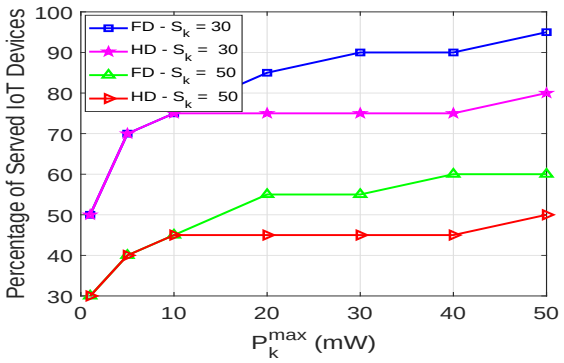

Fig. 9. Percentage of served devices vs. $P_k^{\max}$ with different data size.

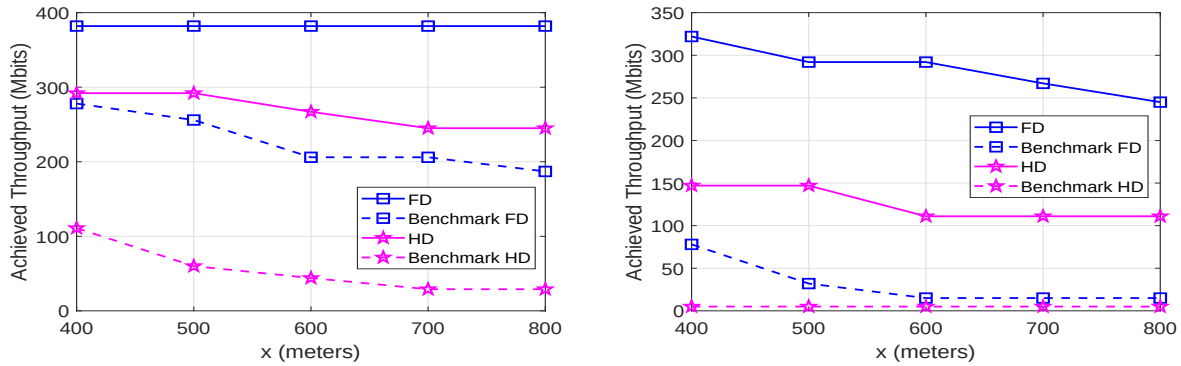

(a) B = 10 (b) B = 5

Fig. 10. Total achievable throughput vs. different network sizes.

lower bounds of FD and HD, respectively. Our proposed algorithms utilize the spectrum more efficiently in comparison to the benchmark schemes with fixed bandwidth allocation. Particularly, in Fig. 3(b), with $x = 1000$ and $N = 60$, the performance of HD is found to be better than the Benchmark FD scheme. It is because the effectiveness of using bandwidth allocation in proposed designs. The results show the superiority of the proposed algorithms over the benchmark schemes.

In Fig. 4, we investigate the performance with different r_{thresh} requirements, where $K = 20$, S_k ranging from 5 to 30 Mbits, $n_{\text{end},k}^{\min} = 50$ time slots, $n_{\text{end},k}^{\max} = 60$ time slots, and N = 70 time slots. Specifically, the QoS is defined as the minimum rate threshold at the UAV/GW to successfully decode the signal, i.e., $r_{1k,\text{thresh}}[n]$ and $r_{2k,\text{thresh}}[n]$. For simplicity, we assume that $r_{1k,\text{thresh}}[n] = r_{2k,\text{thresh}}[n] = r_{\text{thresh}}$. It is observed that the more the minimum rate threshold is required, the fewer users that the system can serve. This is due to the fact that the UAV tends to get closer or spend more time around an IoT device to gain a higher rate requirement. It leads to the UAV having less chance of serving more devices due to

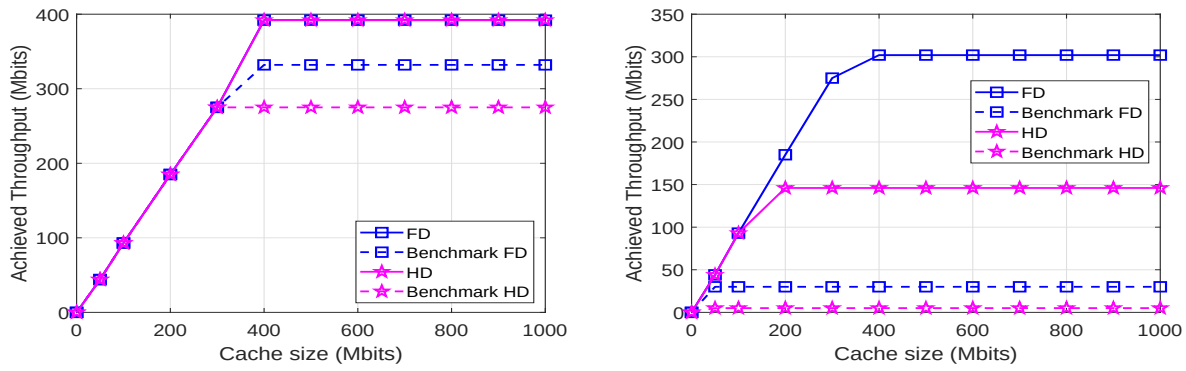

(a) N = 70 (b) N = 60

Fig. 11. Total achievable throughput vs. different cache sizes.

limited flight time and requested timeout constraint at each user. Another observation is that for a larger cache size, the number of served users is increasing. It is due to the fact that the UAV has more capacity to store incoming data. Thus, the UAV can serve more users before offloading information to the GW. Similar to Fig. 3, our proposed FD and HD algorithms achieve much better percentage of served IoT devices compared to the Benchmark FD and HD schemes, respectively. Particularly, the performances of the benchmark schemes stay unaltered with the increasing of r_{thresh}. This is because of the fixed bandwidth allocation for each time slot n in these algorithms. This additionally leads to the fluctuation of data transmission rate values with low variance during time slot n, i.e., $r_{1k}[n]$ and $r_{2k}[n]$. Thus, when the r_{thresh} value is still lower than the average rate of the Benchmark FD and Benchmark HD, the performance is insignificantly influenced. However, if r_{thresh} is large enough, the performance of benchmark schemes will drastically affected.

Fig. 5 shows the impact of different value of $\eta_{\text{end,k}}$ on our system, with $N = 80$, K = 20. It is observed that the percentage of served users increases corresponding to $\eta_{\text{end},k} \in [70, 75]$, $[65, 70]$, $[60, 65]$, $[55, 60]$, respectively. It can be explained on the basis of the constraint (20c), which describes the condition for a successfully served user. Since the total gathering throughput is proportional to the time duration allocated for UL/DL. When the time for UL from IoT devices to UAV is large enough, the number of served users significantly depends on the time allocation for DL from UAV to GW. Furthermore, the time period for DL is calculated as $N - \eta_{\text{end},k}^{\min}$ and $N - \eta_{\text{end},k}^{\max}$ for FD and HD schemes, respectively. We see that the period of time allocated for DL in FD scheme is higher than that in HD scheme such that the performance of FD is outperform the HD one. Specifically, the total number of served users obtained from HD can be equaled to the FD method when the value of $N - \eta_{\text{end},k}^{\max}$ is large enough. For instance, in Figs. 5(a) and 5(b), both proposed methods can serve the maximum number of IoT devices when $\eta_{\text{end},k} \in [55, 60]$

and $C \geq 600$. In this scenario, the UAV should work in HD mode for simplicity of operation in realistic implementation.

In Fig. 6, we investigate the effect of service amount on the system performance, where $K = 20$, $n_{\mathrm{end},k}^{\min} = 60$ time slots, $n_{\mathrm{end},k}^{\max} = 70$ time slots, with N = 80 time slots. As inferred from the results, the FD algorithm significantly improves the percentage of the served IoT devices compared with the HD algorithm for all values of cache size. Specifically, at $S_k = 30$ Mbits and $C = 600$ Mbits, the FD scheme can serve 95% of users in the network while the HD imposes 60% of the served users. Moreover, the performance is degraded by increasing the packet size S_k due to the restriction of available resources assigned for the IoT device/UAV, i.e., $P_U^{\max}$, $P_k^{\max}$, $V_{\max}$, and B. Besides, when the value of cache size is sufficiently large, the successfully served users of all schemes converges to the saturation value. Since the performance is dependent not only on the cache size but also on the resources budget (i.e., bandwidth, power) as well as requested timeout at each device.

Fig. 7 presents the results corresponding to the percentage of served GUs versus $P_U^{\max}$ with variable cache size, while $n_{\mathrm{end},k}^{\min} = 65$ time slots, $n_{\mathrm{end},k}^{\max} = 70$ time slots, and N = 80 time slots. As illustrated, the number of served users is enhanced by increasing the power budget, i.e., $P_U^{\max}$. Moreover, the FD scheme provides a better result in comparison with the HD scheme when $P_U^{\max}$ is small, e.g., $P_U^{\max} < 21$ dBm with $C = 300$ Mbits. Nevertheless, the HD method can obtain the same number of served users as the FD method when $P_U^{\max}$ value is large, e.g., $P_U^{\max} \geq 21$ dBm with $C = 300$ Mbits. This is because the FD mode suffers a residual self-interference together with AWGN which significantly increase the noise power at UAV compared to that of HD. Moreover, the RSI is in linear proportion to the $P_U^{\max}$ as in (8) Thus, when $P_U^{\max}$ is large, the UAV should operate in HD mode since the FD mode requires extra energy which may exceed the system energy budget. It is due to the fact that in FD mode the UAV starts transmit data to GW earlier than in HD mode which is highlighted in Fig. 5. This leads to a higher energy consumption at the UAV when it manoeuvers in the FD mode.

Fig. 8 illustrates the percentage of served devices versus number of IoT devices with different cache sizes, where $H = 50$ meters, $B = 10$ MHz, $N = 80$, $n_{\mathrm{end,k}}^{\min} = 65$ time slots, $n_{\mathrm{end,k}}^{\max} = 70$ time slots, $C =$ 600 Mbits. As the same with Figs. 3 to 9, the percentage of served devices of FD method outperforms the HD scheme. Furthermore, the percentage of served users is reduced by increasing the number of IoT users in the same network area. It is because the restriction of resources (i.e., bandwidth and transmit power allocated for UL and DL) and $V_{\max}$ while more devices are considered. Besides, the percentage of served users will enlarge (as expected) with growing the storage capacity at the UAV or decreasing the packet sizes, as in Figs. 8(a) and 8(b), respectively. Nevertheless, the performance is unchanged for

the HD method with $S_k = 10$ Mbits in Figs. 8(a). It can be explained by the fact that, with $C = 300$ and $S_k = 10$ Mbits, the HD scheme can support up to 30 users but it only serves a lower number of devices due to the limited serving time. Furthermore, one can observe that the UAV serves a lower number of IoT devices with a larger service amount S_k. This is expected since the UAV needs to spend more time and resources to compensate the increase of S_k which is in contradiction with the bandwidth, transmit power, and time limitation.

Fig. 9 presents the percentage of served devices as a function of maximum power budget at each IoT user with different data size, i.e., $P_k^{\max}$. We observe that the performance of the HD scheme is inferior to the FD scheme for various values of $P_k^{\max}$ with a large number of devices, e.g., $K \geq 20$. This is due to the fact that the total allocation time for the DL in HD is lower than that in the FD scheme. Notably, both methods can achieve the same performance when the number of users is small, e.g., $K \leq 10$. Therefore, the UAV should work in HD mode when the network size is small, e.g., $K \leq 10$, in order to reap maximal gains.

B. Throughput Maximization:

Herein, we present the corresponding results for the problem of maximizing the total achieved throughput as in Sections III-D and IV-B. In Fig. 10, the total achieved throughput is presented as a function of network sizes, with $K = 20$, S_k is ranging from 5 to 30 Mbits, and $N = 70$ time slots. We observe that the proposed algorithms significantly improve the throughput performance in comparison with the considered references, for all values of network sizes, i.e., x (meters). Concretely, at B = 10 Mbits and x = 500 meters, the FD algorithm can serve all the devices and the HD algorithm achieves less than 23.56%. Whereas the Benchmark FD and Benchmark HD repsectively impose 67.02% and 15.71% of total data amount. Moreover, all schemes achieve better performance with the increasing of total bandwidth. It is because the higher the bandwidth allocation is, the larger the transmission can be achieved. Particularly, one interesting outcome is that the HD is even better than Benchmark FD which emphasizes the preeminence of the proposed algorithms as compared to the references. It is due to the benefits of optimizing bandwidth allocation.

In Fig. 11, we study the influence of the total traveling time versus the total amount of gathering data, with $K = 20$, S_k ranging from 5 to 30 Mbits. It is observed that the more traveling time is assigned, the higher amount of data can be successfully served. Because the UAV has more time to exchange the information with IoT devices or the GW. This leads to the UAV having more chance of gathering the data. Moreover, all schemes approach their respective saturation point with the increasing values of C, e.g., when $C \geq 400$ Mbits for the FD algorithm. Particularly, at N = 70, the HD scheme can obtain the

same performance as FD one. We conclude that when the total traveling time is sufficient large, the UAV should operate at HD mode for simplicity and reduce the abundant power consumption in comparison to the FD mode.

VI. Conclusion

We investigated the resource allocation and trajectory design for UAV-assisted FD IoT networks with emergency communication system, which take into consideration the latency requirements from concerned IoT devices and the limited storage capacity of the UAV. In this context, we formulated the analytical problem to maximize the total number of served IoT devices via joint optimization of the UAV trajectory, allocated bandwidth, as well as the transmission power for the devices and UAV, while satisfying the requested timeout constraints and storage capacity. Due to the non-convexity of the formulated problem, we transformed the original problem into a tractable form which is then solved using an iterative algorithm having a polynomial computational complexity per iteration. Besides, pertaining to the realistic requirements for improving the estimation accuracy in a natural disaster or emergency scenario, we proposed an additional optimization problem in order to maximize the total collected data while the threshold of minimum number of served IoT devices is guaranteed. We illustrated via numerical results that the proposed designs outperform the benchmark schemes in terms of both total number of served users and the amount of collected data. Particularly, when the RT from all IoT devices is not stringent or in the case of small network size, the UAV should operate in the HD mode for a simple implementation.

Appendix A: Proof of Lemma 2

As in [30, Eq. (20)], we have

$$h_1(x,y,z) \geq \ln\left(1+\frac{x^{(j)}}{y^{(j)}z^{(j)}}\right) - \frac{x^{(j)}}{y^{(j)}z^{(j)}} + 2\frac{\sqrt{x^{(j)}}\sqrt{x}}{y^{(j)}z^{(j)}} - \frac{x^{(j)}\left(x+yz\right)}{y^{(j)}z^{(j)}\left(x^{(j)}+y^{(j)}z^{(j)}\right)}, \tag{A.1}$$

$$h_2(x,z) \geq \ln\left(1+\frac{x^{(j)}}{z^{(j)}}\right) - \frac{x^{(j)}}{z^{(j)}} + 2\frac{\sqrt{x^{(j)}}\sqrt{x}}{z^{(j)}} - \frac{x^{(j)}\left(x+z\right)}{z^{(j)}\left(x^{(j)}+z^{(j)}\right)}. \tag{A.2}$$

By applying (31), the upper bound of yz in (A.1) is given by

$$yz \leq \frac{y^{(j)}}{2z^{(j)}}z^2 + \frac{z^{(j)}}{2y^{(j)}}y^2, \tag{A.3}$$

with $x \geq 0$, $y \geq 0$, $z \geq 0$, $x^{(j)} \geq 0$, $y^{(j)} \geq 0$, $z^{(j)} \geq 0$.

Then, replacing (A.3) into (A.1), we obtain (32) and (33). The Lemma 2 is hence proved.

APPENDIX B

From (A.3), the upper bound of $z_k[n]t_{1k}[n]$ in $r_{1k}^{\mathrm{lb}}[n]$ is:

$$z_k[n]t_{1k}[n] \leq (z_{1k}[n]t_{1k}[n])^{\mathrm{ub}} \triangleq \frac{z_{1k}^{(j)}[n]\,(t_{1k}[n])^2}{2t_{1k}^{(j)}[n]} + \frac{t_{1k}^{(j)}[n]\,(z_{1k}[n])^2}{2z_{1k}^{(j)}[n]}. \tag{B.1}$$

By making use of (32), (33), and (B.1), the lower bound of $\Phi_{1k}[n]$ and $\Phi_{2k}[n]$ are, respectively

$$\begin{aligned}\Phi_{1k}[n] &\geq \bar{\Phi}_{1k}[n] \\ &\triangleq B\Big(A_1 + A_2\big(p_{1k}[n]\big) - A_3\big(p_{1k}[n], t_{1k}[n], z_{1k}[n]\big)\Big),\end{aligned} \tag{B.2}$$

$$\begin{aligned}\Phi_{2k}[n] &\geq \bar{\Phi}_{2k}[n] \\ &\triangleq B\Big(C_1 + C_2\big(p_{2k}[n]\big) - C_3\big(p_{2k}[n], z_{2k}[n]\big)\Big),\end{aligned} \tag{B.3}$$

where

$$A_1 \triangleq \log_2\left(1 + \frac{p_{1k}^{(j)}[n]|\tilde{h}_{1k}[n]|^2\omega_0}{z_{1k}^{(j)}[n]t_{1k}^{(j)}[n]}\right) - \frac{p_{1k}^{(j)}[n]|\tilde{h}_{1k}[n]|^2\omega_0}{z_{1k}^{(j)}[n]t_{1k}^{(j)}[n]\ln 2},$$

$$A_2(p_{1k}[n]) \triangleq |\tilde{h}_{1k}[n]|^2\omega_0 \frac{2\sqrt{p_{1k}^{(j)}[n]}\sqrt{p_{1k}[n]}}{z_{1k}^{(j)}[n]t_{1k}^{(j)}[n]\ln 2},$$

$$\begin{aligned}A_3(p_{1k}[n], t_{1k}[n], z_{1k}[n]) \triangleq{}& \frac{1}{p_{1k}^{(j)}[n]|\tilde{h}_{1k}[n]|^2\omega_0 + z_{1k}^{(j)}[n]t_{1k}^{(j)}[n]} \times \frac{p_{1k}^{(j)}[n]|\tilde{h}_{1k}[n]|^2\omega_0}{z_{1k}^{(j)}[n]t_{1k}^{(j)}[n]\ln 2}\Bigg(p_{1k}[n]|\tilde{h}_{1k}[n]|^2\omega_0 \\ &+ \frac{z_{1k}^{(j)}[n]\,(t_{1k}[n])^2}{2t_{1k}^{(j)}[n]} + \frac{t_{1k}^{(j)}[n]\,(z_{1k}[n])^2}{2z_{1k}^{(j)}[n]}\Bigg),\end{aligned}$$

$$C_1 \triangleq \log_2\left(1 + \frac{p_{2k}^{(j)}[n]|\tilde{h}_{2k}[n]|^2\omega_0}{z_{2k}^{(j)}[n]\sigma^2}\right) - \frac{p_{2k}^{(j)}[n]|\tilde{h}_{2k}[n]|^2\omega_0}{z_{2k}^{(j)}[n]\sigma^2\ln 2},$$

$$C_2(p_{2k}[n]) \triangleq \frac{|\tilde{h}_{2k}[n]|^2\omega_0}{z_{2k}^{(j)}[n]\sigma^2\ln 2} 2\sqrt{p_{2k}^{(j)}[n]}\sqrt{p_{2k}[n]},$$

$$C_3(p_{2k}[n], z_{2k}[n]) \triangleq \frac{p_{2k}^{(j)}[n]|\tilde{h}_{2k}[n]|^2\omega_0}{p_{2k}^{(j)}[n]|\tilde{h}_{2k}[n]|^2\omega_0 + z_{2k}^{(j)}[n]\sigma^2} \times \frac{\Big(p_{2k}[n]|\tilde{h}_{2k}[n]|^2\omega_0 + z_{2k}[n]\sigma^2\Big)}{z_{2k}^{(j)}[n]\sigma^2\ln 2}.$$

REFERENCES

[1] K. Ashton, "That internet of things thing," *RFID journal*, vol. 22, no. 7, pp. 97–114, 2009.

[2] Q. Pham, F. Fang, N. Ha, M. Le, Z. Ding, L. Le, and W. Hwang, "A survey of multi-access edge computing in 5G and beyond: Fundamentals, technology integration, and state-of-the-art," *IEEE Access*, 2019.

[3] Ericsson, "Ericsson mobility report: November 2019," 2019.

[4] S. Yan, M. Peng, and X. Cao, "A game theory approach for joint access selection and resource allocation in UAV assisted IoT communication networks," *IEEE Internet Things J.*, vol. 6, no. 2, pp. 1663–1674, 2018.

[5] Y. Zeng, Q. Wu, and R. Zhang, "Accessing from the sky: A tutorial on UAV communications for 5G and beyond," *P. IEEE*, vol. 107, no. 12, pp. 2327–2375, 2019.

[6] M. Mozaffari, W. Saad, M. Bennis, and M. Debbah, "Unmanned aerial vehicle with underlaid device-to-device communications: Performance and tradeoffs," *IEEE Trans. Wireless Commun.*, vol. 15, no. 6, pp. 3949–3963, Jun. 2016.

[7] W. F. J. Wang, Y. Chen, X. Wang, N. Ge, and J. Lu, "Uav-aided MIMO communications for 5G Internet of Things," *IEEE Internet Things J.*, vol. 6, no. 2, pp. 1731–1740, 2018.

[8] N. Motlagh, M. Bagaa, and T. Taleb, "Energy and delay aware task assignment mechanism for UAV-based IoT platform," *IEEE Internet Things J.*, vol. 6, no. 4, pp. 6523–6536, 2019.

[9] J. W. et al., "Energy-efficient data collection and device positioning in UAV-assisted IoT," *IEEE Internet Things J.*, vol. 7, no. 2, pp. 1122–1139, 2019.

[10] Z. Yuan, J. Jin, L. Sun, K. Chin, and G. Muntean, "Ultra-reliable IoT communications with UAVs: A swarm use case," *IEEE Commun. Mag.*, vol. 56, no. 12, pp. 90–96, 2018.

[11] J. Liu, X. Wang, B. Bai, and H. Dai, "Age-optimal trajectory planning for UAV-assisted data collection," in *IEEE Conf. Computer Commun. Works. (INFOCOM WKSHPS)*, 2018, pp. 553–558.

[12] M. Abd-Elmagid and H. Dhillon, "Average peak age-of-information minimization in UAV-assisted IoT networks," *IEEE Trans. Veh. Technol.*, vol. 68, no. 2, pp. 2003–2008, 2018.

[13] W. Li, L. Wang, and A. Fei, "Minimizing packet expiration loss with path planning in UAV-assisted data sensing," *IEEE Wireless Commun. Lett.*, vol. 8, no. 6, pp. 1520–1523, 2019.

[14] M. Samir, S. Sharafeddine, C. Assi, M. Nguyen, and A. Ghrayeb, "UAV trajectory planning for data collection from time-constrained IoT devices," *IEEE Trans. Wireless Commun.*, vol. 19, no. 1, pp. 34–46, Jan. 2020.

[15] P. S. et al., "Latency critical IoT applications in 5G: Perspective on the design of radio interface and network architecture," *IEEE Commun. Mag.*, vol. 55, no. 2, pp. 70–78, 2017.

[16] D. H. Tran, T. X. Vu, S. Chatzinotas, and B. Ottersten, "Energy-efficient trajectory design for UAV-enabled wireless communications with latency constraints," in *2019 53rd Asilomar Conf. Sig., Sys., and Comp.*, 2019, pp. 347–352.

[17] D. H. Tran, T. X. Vu, S. Chatzinotas, S. ShahbazPanahi, and B. Ottersten, "Coarse Trajectory Design for Energy Minimization in UAV-Enabled," *IEEE Trans. Veh. Tech.*, vol. 69, no. 9, pp. 9483–9496, 2020.

[18] Q. Song, F. Zheng, Y. Zeng, and J. Zhang, "Joint beamforming and power allocation for UAV-enabled full-duplex relay," *IEEE Trans. Veh. Technol.*, vol. 68, no. 2, pp. 1657–1671, 2018.

[19] H. Wang, J. Wang, G. Ding, J. Chen, Y. Li, and Z. Han, "Spectrum sharing planning for full-duplex UAV relaying systems with underlaid D2D communications," *IEEE J. Sel. Areas Commun.*, vol. 36, no. 9, pp. 1986–1999, 2018.

[20] B. Duo, Q. Wu, X. Yuan, and R. Zhang, "Energy Efficiency Maximization for Full-Duplex UAV Secrecy Communication," *IEEE Trans. Veh. Technol.*, vol. 69, no. 4, pp. 4590–4595, 2020.

[21] H. Ye, X. Kang, J. Joung, and Y. Liang, "Optimization for Full-Duplex Rotary-Wing UAV-Enabled Wireless-Powered IoT Networks," *IEEE Trans. Wireless Commun.*, 2020.

[22] B. Marks, "A general inner approximation algorithm for nonconvex mathematical programs," *Oper. Res.*, vol. 26, no. 4, pp. 681–683, 1978.

[23] Y. Zeng, R. Zhang, and T. J. Lim, "Wireless communications with unmanned aerial vehicles: Opportunities and challenges," *IEEE Trans. Commun.*, vol. 54, no. 5, pp. 36–42, May 2016.

[24] A. Osseiran, F. Boccardi, V. Braun, K. Kusume, P. Marsch, M. Maternia, O. Queseth, M. Schellmann, H. Schotten, H.Taoka

et al., "Scenarios for 5G mobile and wireless communications: the vision of the METIS project," *IEEE Commun. Mag.*, vol. 52, no. 5, pp. 26–35, 2014.

[25] S. Gautam, E. Lagunas, S. Chatzinotas, and B. Ottersten, "Relay Selection and Resource Allocation for SWIPT in Multi-User OFDMA Systems," *IEEE Trans. Wireless Commun.*, vol. 18, no. 5, pp. 2493–2508, 2019.

[26] Y. Yuan, L. Lei, T. X. Vu, S. Chatzinotas, S. Sun, and B. Ottersten, "Energy minimization in UAV-aided networks: actor-critic learning for constrained scheduling optimization," *in Arxiv*, preprint arXiv:2006.13610.

[27] S. Gong, S. Wang, C. Xing, S. Ma, and T. Q. Quek, "Robust Superimposed Training Optimization for UAV Assisted Communication Systems," *IEEE Trans. Wireless Commun.*, pp. 1704 – 1721, Mar. 2020.

[28] V. D. Nguyen, H. V. Nguyen, O. A. Dobre, and O. S. Shin, "A new design paradigm for secure full-duplex multiuser systems," *IEEE J. Select. Areas Commun.*, vol. 36, no. 7, pp. 1480–1498, July 2018.

[29] A. Sabharwal, P. Schniter, D. Guo, D. W. Bliss, S. Rangarajan, and R. Wichman, "In-band full-duplex wireless: Challenges and opportunities," *IEEE J. Select. Areas Commun.*, vol. 32, no. 9, pp. 1637–1652, Feb. 2014.

[30] V. D. Nguyen, T. Q. Duong, H. D. Tuan, O. S. Shin, and H. V. Poor., "Spectral and energy efficiencies in full-duplex wireless information and power transfer," *IEEE Trans. Commun*, vol. 65, no. 5, pp. 2220–2233, May 2017.

[31] H. V. Nguyen, V. D. Nguyen, O. A. Dobre, Y. Wu, and O. S. Shin, "Spectral and energy efficiencies in full-duplex wireless information and power transfers," *IEEE Trans. Wireless Commun.*, vol. 18, no. 6, pp. 2946–2963, June 2019.

[32] M. Duarte, C. Dick, and A. Sabharwal, "Experiment-driven characterization of full-duplex wireless systems," *IEEE Trans. Wireless Commun.*, vol. 11, no. 12, pp. 4296–4307, Dec. 2012.

[33] N. Dan, T. Le-Nam, P. Pekka, and L. Matti, "On the spectral efficiency of full-duplex small cell wireless systems," *IEEE Trans. Wireless Commun.*, vol. 13, no. 9, pp. 4896–4910, 2014.

[34] U. Challita, W. Saad, and C. Bettstetter, "Interference management for cellular-connected UAVs: A deep reinforcement learning approach," *IEEE Trans. Wireless Commun.*, vol. 18, no. 4, pp. 2125–2140, April 2019.

[35] T. S. Rappaport, *Wireless communications: principles and practice*. prentice hall PTR New Jersey, 1996, vol. 2.

[36] V. S. Abhayawardhana, I. J. Wassell, D. Crosby, M. P. Sellars, and M. G. Brown, "Comparison of empirical propagation path loss models for fixed wireless access systems," in *Proc. IEEE 61st Veh. Technol. Conf.*, vol. 1, 2005, pp. 73–77.

[37] A. Beck, A. Ben-Tal, and L. Tetruashvili, "A sequential parametric convex approximation method with applications to nonconvex truss topology design problems," *J. Global Optim.*, vol. 47, no. 1, pp. 29–51, May 2010.

[38] S. Boyd and L. Vandenberghe, *Convex optimization*. Cambridge University Press, 2004.

[39] B. Ashok, B. S. Mysore, S. Chatzinotas, and B. Ottersten, "A joint solution for scheduling and precoding in multiuser MISO downlink channels," *IEEE Trans. Wireless Commun.*, vol. 19, no. 1, pp. 475–490, Jan. 2019.

[40] S. Boyd, "Advances in convex optimization: Interior-point methods, cone programming, and applications," 2002.

[41] Y. Zeng, J. Xu, and R. Zhang, "Energy minimization for wireless communication with rotary-wing UAV," *IEEE Trans. Wireless Commun.*, vol. 18, no. 4, pp. 2329–2345, April 2019.